

RESEARCH ACTIVITIES IV

Department of Molecular Assemblies

IV-A Solid State Properties of Phthalocyanine Salts and Related Compounds

Some phthalocyanine molecules contain unpaired d-electrons in the conjugated π -electron system. Due to this special nature, the itinerant π -electrons and localized unpaired d-electrons coexist in solid phthalocyanine salts, in which a one-dimensional double-chain system (metal and ligand chain) is formed. Furthermore these chains make up wide (π -band) and narrow (d-band) one-dimensional bands, the energy of the narrow band being close to the Fermi energy of the wide band. The phthalocyanine conductor is thus a two-chain and two-band system. The exchange interaction of itinerant π -electrons with localized magnetic moments is a new aspect in the field of organic metals. For the sake of basic understanding of these materials, where a magnetic interaction takes an important role, we prepare and characterize the solid phthalocyanine salts and related compounds.

IV-A-1 ESR Properties of Oriented Single Crystals of $\text{Co}_x\text{Ni}_{1-x}\text{Pc}(\text{AsF}_6)_{0.5}$

SIMONYAN, Mkhitar; YONEHARA, Yukako¹;
DING, Yuqin¹; YAKUSHI, Kyuya
(¹GUAS)

Phthalocyanine conductor $\text{CoPc}(\text{AsF}_6)_{0.5}$ has two magnetic subsystems: the localized 3d-electron of Co and itinerant π -electron of Pc. However, this compound is ESR silent, since the spin-orbit interaction in Co and dipole-dipole interaction between molecules are strong. The magnetically diluted system $\text{Co}_x\text{Ni}_{1-x}\text{Pc}(\text{AsF}_6)_{0.5}$ is formed by mixing $\text{CoPc}(\text{AsF}_6)_{0.5}$ in non-magnetic nearly isostructural $\text{NiPc}(\text{AsF}_6)_{0.5}$. When $x = 0.01$, we found an anisotropic hyperfine structure at 3.2 K. From the angular dependence of the hyperfine structure, the hyperfine constants and principal g -values are determined as $A = 0.017 \text{ cm}^{-1}$, $B = 0.032 \text{ cm}^{-1}$, $g_{\parallel} = 2.056$, and $g_{\perp} = 3.045$ at 3.2 K. The hyperfine constants A and B are very close to those of insulating mixed crystal $\text{Co}_{0.001}\text{Ni}_{0.999}\text{Pc}$ but the g -values are very different between them, which means the different electronic state in Co 3d-orbital. In contrast to $\text{Co}_{0.001}\text{Ni}_{0.999}\text{Pc}$, the ESR signal of $\text{Co}_{0.01}\text{Ni}_{0.99}\text{Pc}(\text{AsF}_6)_{0.5}$ shows strong temperature dependence. As shown in Figure 1, the hyperfine structure collapse into a single Lorentzian line above 40 K, the metal-insulator transition temperature. This is direct evidence that the conduction electrons in ligand (Pc) site are interacting with the local magnetic moment of Co site. This exchange interaction is strongly reflected on the temperature dependence of g_{\perp} as well.

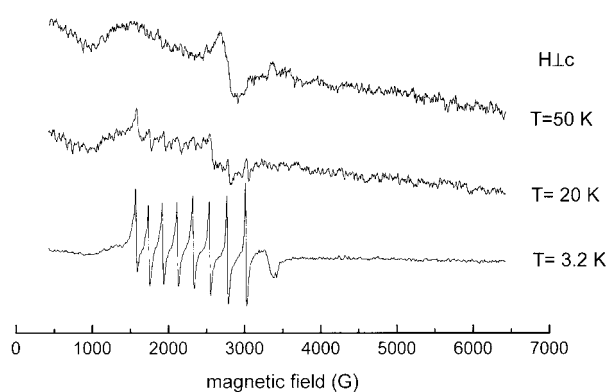


Figure 1. Hyperfine structure of the ESR signal of $\text{Co}_{0.01}\text{Ni}_{0.99}\text{Pc}(\text{AsF}_6)_{0.5}$ at 3.2 K. Above 40 K, in a metallic phase, this hyperfine structure collapse into a single Lorentzian through the exchange coupling with itinerant π -electrons.

IV-A-2 Pressure-Temperature Phase Diagram of $\text{NiPc}(\text{AsF}_6)_{0.5}$

SIMONYAN, Mkhitar; YAKUSHI, Kyuya

We have shown before that $\text{NiPc}(\text{AsF}_6)_{0.5}$ shows a continuous charge transfer from the metal 3d-band to the ligand π -band and this charge transfer begins at 1 GPa.^{1,2)} From the analysis of the plasmon absorption band, we predicted that a metal-insulator (MI) transition accompanied this continuous charge transfer phenomenon. It is therefore expected that the MI transition occurs at the same pressure, *ca.* 1 GPa, at room temperature. On the other hand this compound undergoes a MI transition around 40 K at ambient pressure. This observation suggests that the temperature of this MI transition will increase from 40 K to room temperature when the high-pressure is applied to this compound. Figure 1 actually realizes our expectation: the resistance minimum monotonously increases up to 283 K at 0.95 GPa. The insulator phase of $\text{NiPc}(\text{AsF}_6)_{0.5}$ brought about by the 3d- π charge transfer is likely to be a state of Anderson localization. The mechanism of this MI transition is unique among the organic conductors.

References

1) T. Hiejima and K. Yakushi, *J. Chem. Phys.* **103**, 3950 (1995).

2) Y. Yonehara and K. Yakushi, *Synth. Met.* **94**, 149 (1998).

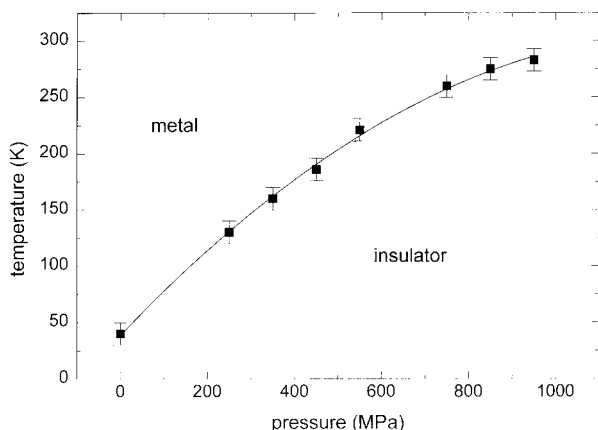


Figure 1. P-T Phase diagram of NiPc(AsF₆)_{0.5}: The squares represent the resistivity-minimum temperature against the pressure. Note that the insulator phase expands according to the pressure, which is associated with the continuous charge-transfer phenomenon.

IV-A-3 New Raman Bands Found in the Mixed Crystals of Ni_{1-x}Co_xPc(AsF₆)_{0.5}

YONEHARA, Yukako¹; DING, Yuqin¹; SIMONYAN, Mkhitar; YAKUSHI, Kyuya
(¹GUAS)

We show by X-ray diffraction and EPMA that the nearly isostructural NiPc(AsF₆)_{0.5} and CoPc(AsF₆)_{0.5} make mixed crystals Ni_{1-x}Co_xPc(AsF₆)_{0.5} in a wide range of x ($1 \geq x \geq 0$). We find new Raman bands at 370 cm⁻¹ and 740 cm⁻¹ that appear only in the mixed crystals, when the He-Ne laser (632.8 nm) is polarized parallel to the c -axis (conducting axis). The symmetry of these Raman modes is a_{1g} , since they appear in the configuration of $b(c,c)-b$ or $a(c,c,-a)$. When we change the excitation light to Ar⁺ laser (514.5 nm), these new Raman bands are remarkably weakened or disappear. This suggests the resonance effect for the appearance of the new bands, thereby new excited state is formed around 15×10^3 cm⁻¹ in the mixed crystals and the transition moment to this excited state is parallel to the c -axis. This excited state is proposed to be a charge-transfer state from the filled $3d_{z^2}$ -orbital of NiPc to the partly vacant $3d_{z^2}$ -orbital of CoPc. The 370 cm⁻¹ and its overtone mode 740 cm⁻¹ are associated with the deformation mode of isoindole ring.

IV-B Structure and Properties of Organic Conductors

The study of organic metals rapidly developed when the dimensionality of an intermolecular charge-transfer interaction is expanded. This expansion of dimensionality has been brought about by the discovery of new molecules such as BEDT-TTF or C₆₀. The most basic physical parameters are the transfer integrals that represent the dimensionality and itinerancy of the electron, and the on-site Coulomb energy and coupling constants with molecular vibration, which represent the localized character of the electron. We systematically determine these parameters by polarized reflection spectroscopy assembling a microscope, multi-channel detection system, FT-IR, and liquid helium cryostat.

Another ongoing program is to look for negative- U organic charge-transfer compounds, the strategy of which is described in the special research project of this issue. In this research program, the most important parameter is the charge or valence of the molecule in a mixed-valent state. The examination of the electronic and vibrational spectra at low temperature or high pressure is most efficient to characterize the valence. Molecular metals consisting of large or long molecules are examined by reflection and Raman spectroscopy at low temperature.

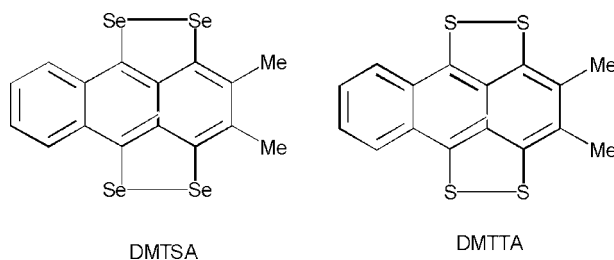
IV-B-1 Spectroscopic Study of Isostructural Charge-Transfer Salts: Non-Metallic DMTTA-BF₄ and Metallic DMTSA-BF₄

OUYANG, Jianyong¹; DONG, Jian¹; YAKUSHI, Kyuya; TAKIMIYA, Kazuo²; OTSUBO, Tetsuo²
(¹GUAS; ²Hiroshima Univ.)

[*J. Phys. Soc. Jpn.* in press]

We present the polarized reflection spectra of non-metallic DMTTA-BF₄ and the isostructural metallic DMTSA-BF₄. From these spectra, both compounds were regarded as quasi-one-dimensional conductors. From the analysis of these spectra we show that DMTTA-BF₄ is a Mott insulator with $U/4t \sim 0.8-1.2$ and DMTSA-BF₄ is a weakly correlated metal with structural fluctuation near the room temperature. Resistivity, thermopower, and ESR are consistent with the above picture, and demonstrate the phase transitions at *ca.* 100 K for DMTTA-BF₄ and at *ca.* 150 K for DMTSA-BF₄. The low-temperature reflection spectra of

both compounds strongly suggest the breaking of screw-axis symmetry along the conducting axis. These phase transitions are regarded as the spin Peierls transition (DMTTA-BF₄) and Peierls (DMTSA-BF₄) transition. Assuming a dimerized stack, we estimate the transfer integrals t_1 and t_2 as 0.25 and 0.21 eV from the 10 K spectrum of DMTSA-BF₄. The coupling constants of molecular vibration of DMTSA with the inter-molecular charge-transfer excitation are obtained analyzing the polarized reflection spectrum of DMTSA-ClO₄ having a dimerized structure.



IV-B-2 Suppression of the Metal-Insulator Transition under High Pressure in 1:1 Metallic DMTSA-BF₄

SIMONYAN, Mkhitar; YAKUSHI, Kyuya; TAKIMIYA, Kazuo¹; OTSUBO, Tetsuo¹
(¹Hiroshima Univ.)

DMTSA-BF₄ undergoes a metal-insulator transition of a Peierls type.¹⁾ This phase transition is suppressed by applying 400 MPa as shown in the figure. Probably the inter-chain transfer integral t_{ab} is enhanced by the high pressure. Taking t_{ab} into account, we have examined the band structure of this compound. However, this transfer integral provides no change in one-dimensional Fermi surface, if the band is half-filled. The high-pressure experiment requires the further examination of the band-filling factor or inter-chain coupling through the counter anion BF₄.

We have measured the resistance of 500 MPa down to 0.23 K using the ³He cryostat equipped in the Molecular Materials Center. However, superconductivity was not found in this compound at this pressure. All organic compound which shows superconductivity has TTF skeleton. This might suggest that the high-frequency phonon structure is associated with the mechanism of the superconductivity in organic superconductor.

Reference

- 1) J. Dong, K. Yakushi, K. Takimiya and T. Otsubo, *J. Phys. Soc. Jpn.* **67**, 971 (1998).

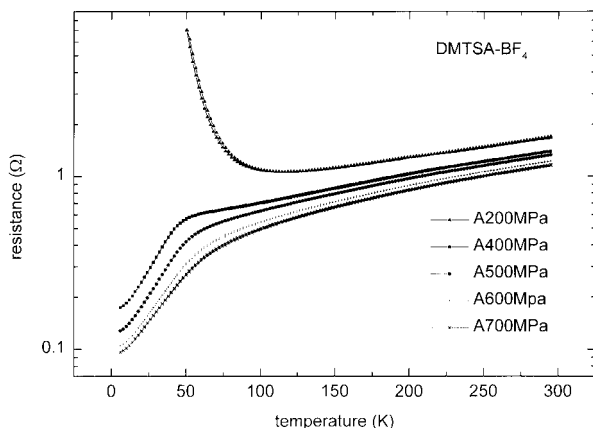


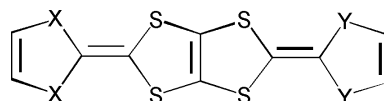
Figure 1. Temperature dependence of the resistance of DMTSA-BF₄. The metallic state is maintained at least down to 2 K above 400 MPa.

IV-B-3 Band Structure of Organic Metals (BDT-TTP)₂X (X = ClO₄, ReO₄), (ST-TTP)₂AsF₆, and (BDS-TTP)₂AsF₆ Studied by Reflection Spectroscopy

OUYANG, Jianyong¹; YAKUSHI, Kyuya; MISAKI, Yohji²; TANAKA, Kazuyoshi²
(¹GUAS; ²Kyoto Univ.)

The charge-transfer salts of BDT-TTP with β -type molecular arrangement have quasi-one-dimensional metallic band. We have experimentally determined the

intra (t_a)- and inter-chain (t_p) transfer integrals of (BDT-TTP)₂X (X = AsF₆, SbF₆)_{0.5}. We apply the same spectroscopic method to the title compounds. (ST-TTP)₂AsF₆ and (BDS-TTP)₂AsF₆ are isostructural to (BDT-TTP)₂SbF₆ with P1 space group. The transfer integrals are $t_a = -0.24$ eV, $t_p = -0.042$ eV for (ST-TTP)₂AsF₆ and $t_a = -0.26$ eV, $t_p = -0.044$ eV for (BDS-TTP)₂AsF₆. These values are not significantly enhanced compared with (BDT-TTP)₂X (X = AsF₆, SbF₆), although selenium atoms are introduced at the outer sulfur position. Probably the increase of the overlap between selenium-sulfur orbitals is compensated by the decrease of the sulfur-sulfur overlap. This system became more anisotropic at low temperatures as well as (BDT-TTP)₂X (X = AsF₆, SbF₆). (BDT-TTP)₂X (X = ClO₄, ReO₄) are isostructural to each other with the space group of C2/c. The intra-chain (t_b) and inter-chain (t_p) transfer integrals are estimated as $t_b = 0.26$ eV, $t_p = -0.048$ eV for ClO₄ salt and $t_b = 0.25$ eV, $t_p = -0.047$ eV for ReO₄ salt. From the spectral data we corrected the chemical ratio of ReO₄ salt as 2:1, although it was reported as (BDT-TTP)₂(ReO₄)_{0.72}. We analyze the reflectivity curve $R(\omega)$ using generalized Drude model and find $R(\omega)$ along the inter-chain direction deviates significantly from the simple Drude model.



X = Y = S: BDT-TTP
X = S, Y = Se: ST-TTP
X = Y = Se: BDS-TTP

IV-B-4 Insulator-Insulator Phase Transition of θ -(BDT-TTP)₂Cu(NCS)₂: Strongly Correlated Two-Dimensional System

OUYANG, Jianyong¹; YAKUSHI, Kyuya; MISAKI, Yohji²; TANAKA, Kazuyoshi²
(¹GUAS; ²Kyoto Univ.)

Contrary to the metallic properties of β -type (BDT-TTP)₂X, θ -type (BDT-TTP)₂Cu(NCS)₂ is an insulator, although a simple tight-binding calculation leads to a two-dimensional metallic band. A phase transition is found at 250 K in the electrical resistance measurement, the activation energy being changed from 30-40 meV (HT phase) to 100 meV (LT phase). The spin susceptibility changes the temperature dependence at 250 K, below which it conforms to a Curie-Weiss law with $C = 0.143$ and $\theta = 19$ K. Although this magnetic property is not well understood, it is safely concluded that the charge on BDT-TTP is rather localized in the LT phase. The reflectivity exhibits the so-called charge-transfer (CT) band in two polarization directions, which means the inter-molecular interaction is two-dimensional. This CT band dramatically changes at the phase transition temperature, increasing the gap energy below the phase transition temperature. This behavior strongly suggests the structural change through the phase transition, although the LT phase structure is not known. As shown in the figure, the Raman spectrum of the C=C stretching mode has an asymmetric broad lineshape in HT phase.

It shows a complicated splitting accompanied by the appearance of new peaks below the phase transition temperature. This splitting may be associated with the charge disproportionation.

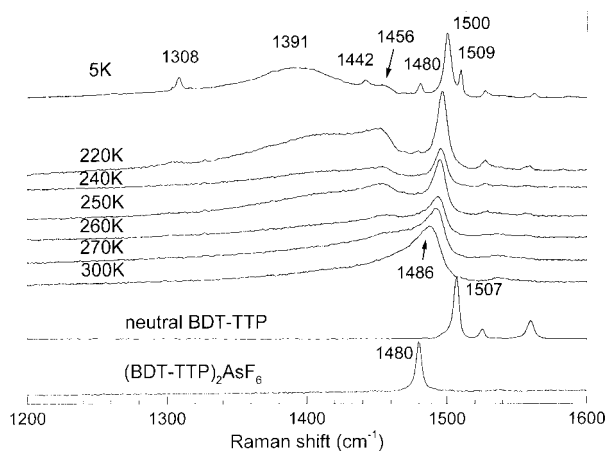


Figure 1. Temperature dependence of the Raman spectrum of C=C stretching mode in θ -(BDT-TTP) $_2$ Cu(NCS) $_2$ along with the room-temperature spectrum of BDT-TTP and (BDT-TTP) $_2$ AsF $_6$ crystals. This charge-sensitive mode continuously changes during the phase transition.

IV-B-5 Phase Transition in Narrow-band Organic Metals (BEDT-ATD) $_2$ X(solvent) (X = PF $_6$, AsF $_6$, BF $_4$; solvent = THF, DHF, DO)

YAKUSHI, Kyuya; URUICHI, Mikio; YAMASHITA, Yoshiro

[*Synth. Met.* in press]

We present the metal-insulator (MI) transition of the title compounds examined by reflection spectroscopy, X-ray diffraction, and magnetic susceptibility. Below the MI transition temperature, the space group changes from $P2_1/a$ to Pa with $4k_F$ lattice modulation in (BEDT-ATD) $_2$ PF $_6$ (DHF) and (BEDT-ATD) $_2$ BF $_4$ (THF) which undergo MI transitions at 150 K and 200 K, respectively. On the other hand, the symmetry change is not observed at about 80 K in (BEDT-ATD) $_2$ PF $_6$ (DO) ($T_{MI} = 100$ K), (BEDT-ATD) $_2$ PF $_6$ (THF) ($T_{MI} < 50$ K), and (BEDT-ATD) $_2$ AsF $_6$ (THF) ($T_{MI} < 50$ K). The $4k_F$ lattice modulation is supported by the magnetic susceptibility experiment as well. The precursor phenomenon of this structural change is observed already at room temperature in (BEDT-ATD) $_2$ PF $_6$ (DO). All of these data suggest the view that (BEDT-ATD) $_2$ X(solvent) is a strongly correlated 1D metal.

The breaking of the center of symmetry in several solvent-containing crystals requires that asymmetric solvents are aligned ferroelectrically below the MI transition temperature as shown in the figure. This suggests the possibility of the ferroelectric state just below the phase transition temperature. The experiment to examine this unusual possibility is now in progress.

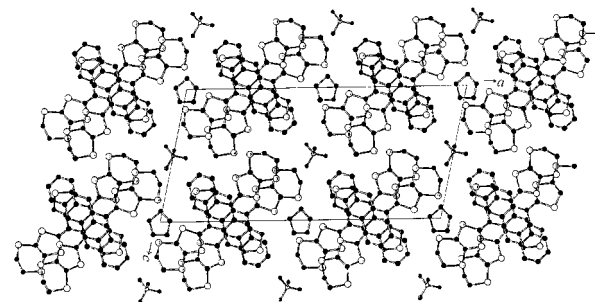
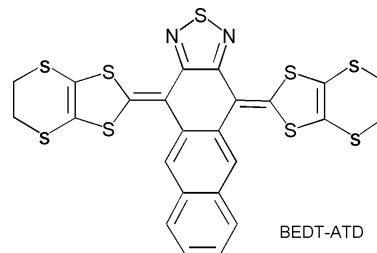


Figure 1. Low-temperature crystal structure of (BEDT-ATD) $_2$ BF $_4$ (THF).

IV-B-6 Experimental and Theoretical Estimation of the Site-Energy Difference in Et $_4$ N(DMTCNQ) $_2$

NAKANO, Chikako; YAKUSHI, Kyuya; UEDA, Kazushi¹; SUGIMOTO, Toyoshige¹
(¹Osaka Pref. Univ.)

[*Chem. Phys. Lett.* in preparation]

DMTCNQ forms a dimerized stack in (Et $_4$ N)-(DMTCNQ) $_2$ with two crystallographically independent sites. Although the average charge of DMTCNQ is -0.5 , the charge in different site has a different value such as $-0.5 + \delta$ and $-0.5 - \delta$. We have estimated this δ as 0.1 by the Raman spectroscopy. The different charge on the non-equivalent site comes from the site-energy difference in the unit cell. This kind of charge disproportionation is sometimes accompanied by the phase transition in organic conductors such as (DI-DCNQI) $_2$ -Ag and α' -(BEDT-TTF) $_2$ IBr $_2$ and is attracting an attention as a new ground state. The pattern of the charge distribution is not only determined by the repulsive force between the adjacent localized charges but also by the electrostatic force with counter anion/cation. Following the last year's experimental work, we conducted the numerical calculation of the Madelung energy, which brings about the site-energy difference. We first calculate the charge distribution in DMTCNQ 0 , DMTCNQ $^-$, and Et $_4$ N $^+$ using the PM3 semi-empirical method in the HyperChem-R5.1 program system. The infinite sum of the electrostatic energy between these point charges is calculated using the Ewald method. The site-energy difference is calculated as 0.14 eV. On the other hand, this site energy difference is estimated based on the ion-neutral dimer model analyzing the reflection and Raman spectra. It is experimentally estimated as 0.082 eV. The agreement with numerical estimation is satisfactory.

IV-B-7 κ' -(ET)₂Cu₂(CN)₃—Superconductor with Mixed Cu₂(CN)₃ and N(CN)₂ Ligands in the Anion Layer Studied by Polarized Reflection Spectroscopy

DROZDOVA, Olga¹; YAKUSHI, Kyuya; SAITO, Gunzi¹; OOKUBO, Kenji¹; YAMOCHI, Hideki¹; KONDO, Tetsuo; URUICHI, Mikio; OUAHAB, Lahcène²

(¹Kyoto Univ.; ²Univ. Rennes)

Since the first discovery of (ET)₂Cu₂(CN)₃ with κ -type donor packing, controversial results were reported concerning its conducting properties. “ κ ” Abbreviation was introduced to distinguish an ambient pressure superconductor with $T_c = 3.8$ K from the semiconductor “ κ' ” with $E_a = 0.04$ – 0.05 eV. The same preparation conditions give the 11.2 K superconductor κ -(ET)₂Cu(CN)[N(CN)₂]. Polarized reflection spectra were measured on the conductive (*bc*) plane of κ -(ET)₂Cu₂(CN)₃, κ' -(ET)₂Cu₂(CN)₃ and κ -(ET)₂Cu(CN)-[N(CN)₂]. Despite the overall similarity of the spectra at 293 K, clear difference in the 2100–2300 cm⁻¹ range was observed. Namely, κ' -(ET)₂Cu₂(CN)₃ exhibits CN stretching peaks characteristic for both κ -(ET)₂Cu₂(CN)₃ and κ -(ET)₂Cu(CN)[N(CN)₂]. Thus anion layer of κ' is regarded as mixture of Cu₂(CN)₃ and Cu(CN)-[N(CN)₂] anions. The mixing ratio was estimated as 2:1 in most samples. Angle dependence suggested that the orientation of the original features conserved within the anion layer of κ' . Homogeneity of the mixing was supported by Raman spectroscopy. Temperature evolution of the reflection spectra followed conducting properties. The chemical formula of κ' -(ET)₂Cu₂(CN)₃ was modified to κ -(ET)₂Cu^{+(2-x-y)}Cu^{2+x}(CN)_(3-2y)-[N(CN)₂]_y, where $x < 0.01$ and $0.1 \leq y \leq 0.8$.

IV-B-8 Raman-active C=C Vibrations of κ -(BEDT-TTF)₂Cu[N(CN)₂]Br and Its Deuterated Analogues

MAKSIMUK, Mikhail; YAKUSHI, Kyuya; KAWAMOTO, Atsushi¹; TANIGUCHI, Hiromi²; KANODA, Kazushi²

(¹Hokkaido Univ.; ²Tokyo Univ.)

The set of progressively deuterated isotopic analogues of κ -(BEDT-TTF)₂Cu[N(CN)₂]Br lies on the border between metals and insulators. Below 80 K, a crystal volume is divided into a metallic phase and an insulating one. The amount of the latter increases with deuteration and depends on the cooling rate near 80K. These crystals have several anomalies in temperature dependencies of their various physical properties. We studied d[0,0], d[2,2], d[3,3] and d[4,4] single crystals, the numbers being the numbers of deuterium atoms in every end of a BEDT-TTF molecule. The C=C stretching modes in resonance Raman spectra (laser wavelength 514.5 nm) have been measured at temperatures between 4.2 and 300 K. In d[2,2], d[3,3] and d[4,4], four modes have been observed: well-known totally symmetric ν_2 , ν_3 ; vibronically coupled $\nu_{27}^-(B_{1u})$ and a mode near 1463 cm⁻¹ (at 5 K) which we assign to $\nu_{27}^+(B_{1u})$. In d[0,0] below 200K, in addition to that, it

has been possible to resolve dimer-dimer splitting of ν_2 and ν_3 . ν_2 and ν_3 have different temperature dependence of this splitting. In d[2,2] all ν_{27}^- parameters and the width of ν_2 depend on the cooling rate near 80 K as well as they are sample-dependent. In both cases it can be explained as the influence of the electronic system: for ν_{27}^- by electron-molecular vibration coupling and for ν_2 width by a change of the dimer-dimer splitting.

IV-B-9 Determination of the Charge on BEDO-TTF in Its Complexes by Raman Spectroscopy

DROZDOVA, Olga¹; YAMOCHI, Hideki¹; YAKUSHI, Kyuya; URUICHI, Mikio; HORIUCHI, Sachio; SAITO, Gunzi¹

(¹Kyoto Univ.)

[*J. Am. Chem. Soc.* submitted]

Raman spectroscopy was employed as a fast and exact method to determine the charge on BEDO-TTF (BO) in its complexes. Linear dependencies between two totally symmetric C=C stretching modes (ν_2 : ring C=C and ν_3 : central C=C) and charge on BO were found and used to evaluate the charge transfer (CT) degree. The CT degree was evaluated by the following equation.

$$\rho = (1524.9 - \nu_{3,\text{obs}} (\text{cm}^{-1}))/109.0$$

$$\rho = (1660.8 - \nu_{2,\text{obs}} (\text{cm}^{-1}))/74.1$$

Using the above equation, 19 complexes, including single crystals, powders and films were examined for the first time. The border between neutral (insulating) and partially CT (conducting) complex based on BO was estimated as 0.3.

IV-B-10 Re-examination of Bromide, Chloride and Iodide Salts of Bis(ethylenedioxy)tetra-thiafulvalene (BEDO-TTF) by Spectroscopic Methods

ULANSKI, Jacek; YAKUSHI, Kyuya; URUICHI, Mikio; DROZDOVA, Olga¹; YAMOCHI, Hideki¹; SAITO, Gunzi¹

(¹Kyoto Univ.)

[*J. Phys. B: Condens. Matter* in preparation]

Recent results of polarized reflectivity, absorption and Raman spectroscopic studies of (BEDO-TTF)₂Br·(H₂O)₃, (BEDO-TTF)₂·4I₃, and (BEDO-TTF)₂Cl·(H₂O)₃ salts are summarized and analyzed. The experimentally obtained plasma frequencies and transfer integrals are considerably smaller than the theoretical values calculated including 3d orbitals; the theoretical calculations neglecting the sulfur 3d orbitals yield more realistic band structure. The polarized reflectance and optical conductivity spectra of the investigated BEDO-TTF salts in the direction perpendicular to the conducting plane reveal some unique features: very strong vibrational bands which originate from vibrations of BEDO-TTF molecules, and in some cases new bands around 5000 cm⁻¹ due to directional dispersion. Detailed analysis of the bands in the range 3200–3500 cm⁻¹ shows that the compositions of the chloride and of

the bromide salts are still not clear in respect to possible presence of the hydroxonium ions and to the role of water molecules. The BEDO-TTF salts containing water molecules are not stable in vacuum, losing both water and anion molecules, what should be taken into account in further investigations of these materials. The absorption spectra for thin, semitransparent single crystal of BEDO-TTF bromide salt, taken at different angles of incident light, demonstrate that the high transparency is due to specific orientation of the BEDO-TTF molecules.

IV-B-11 First Observation of the Plasmon Absorption by Reflection Spectroscopy in the Single Crystal of Two-dimensional Organic Metal

YAKUSHI, Kyuya; ULANSKI, Jacek; YAMOCHI, Hideki¹; SAITO, Gunzi¹
(¹Kyoto Univ.)

Plasmon cannot be detected by the optical absorption method, since it is a longitudinal excitation. However, it becomes detectable in an anisotropic material, if the wave vector of light is not parallel to the principal axis of the anisotropic material. We present the observation and simulation of the plasmon by the method of normal incidence reflection spectroscopy in two-dimensional organic metals $\text{BO}_2\text{Cl}(\text{H}_2\text{O})_3$ and $\text{BO}_{2.4}\text{I}_3$. The plasmon was observed in the specular reflection normal to (111) and $(11\bar{1})$ crystal faces, which respectively make angles of 71.0° and 78.7° with conducting sheet in $\text{BO}_2\text{Cl}(\text{H}_2\text{O})_3$, and that to the $(\bar{1}01)$ crystal face, which makes an angle of 67.0° with the conducting sheet in $\text{BO}_{2.4}\text{I}_3$. The plasmon spectrum is theoretically reproduced solving the Fresnel equation with the principal dielectric function for a two-dimensional metal. We have given the analytical solution of the two-dimensional case. In both cases, the theoretical prediction agrees very well with the observation of the reflectivity at each crystal face. This is the first observation of the plasmon in organic metals. Incidentally, this is physically the same phenomenon as the directional dispersion in an exciton absorption of organic dye.

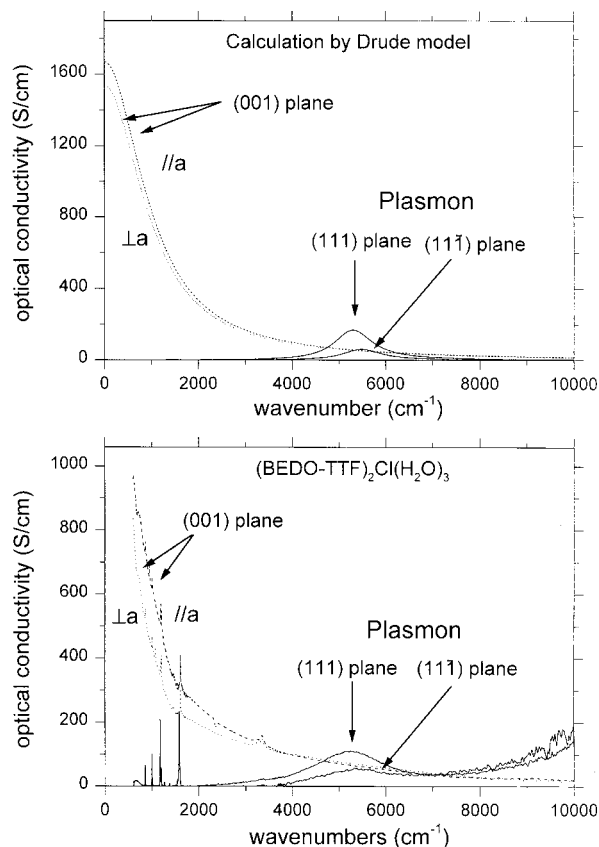


Figure 1. Observed and calculated conductivity spectra in the principal directions //a and $\perp a$ on the (001) conducting plane and non-principal directions on (111) and $(11\bar{1})$ plane in the crystal of $\text{BO}_2\text{Cl}(\text{H}_2\text{O})_3$. Plasmon peak appears at $5000\text{--}6000\text{ cm}^{-1}$ in the spectra on the (111) and $(11\bar{1})$ planes.

IV-C Microscopic Investigation of Molecular-Based Conductors

One of the most remarkable features of molecular-based conductors is taking various electronic phases. Especially, the competition of the ground states is one of the crucial problems of them. Although detailed electronic structure of them are not clear so far, these curious behaviors are believed to be originated from their characteristic natures; highly electronic correlation.

To clarify the low temperature electronic states, we performed the static susceptibility, EPR, ^1H - and ^{13}C -NMR measurements for molecular based conductors.

IV-C-1 Low-Temperature Electronic States in θ -(BEDT-TTF) $_2$ RbZn(SCN) $_4$: Competition of Different Ground States

NAKAMURA, Toshikazu; MINAGAWA, Waka¹; KINAMI, Ryoji¹; KONISHI, Yukihiko¹; TAKAHASHI, Toshihiro¹
(¹Gakushuin Univ.)

[*Synth. Met.* **103**, 1898 (1999)]

Magnetic properties of θ -(BEDT-TTF) $_2$ RbZn(SCN) $_4$ were studied. The compounds of this family are expected to be 2D-metals with a quarter-filled band. However the title salt undergoes a M-I transition around 190 K. The mechanism of the M-I transition and the low-temperature electronic states of the θ -type are not known. To clarify the electronic states of the low-temperature non-metallic phase and the mechanism of the M-I transition, we performed SQUID, EPR, ^1H - and ^{13}C -NMR measurements.

The low temperature behavior of the spin susceptibility, χ_{spin} , was found to depend on the cooling speed around 190 K. The EPR linewidth, ΔH_{pp} , analyses show that a phase transition exists around 190 K, and that the electronic state realized by the rapid-cooling is a metastable state. In the case of slow-cooling, the electron spin concentration exponentially decreases through the formation of spin-gap, and only residual spins concern the NMR relaxation. In the case of rapid-cooling, a large enhancement of the NMR- T_1^{-1} was observed below 90 K where the χ_{spin} shows an abrupt increase. These facts suggest that the NMR relaxation is caused by dilute local magnetic moments. The quenched state may be understood as a new-type charge localization. A small amount of chemical doping caused pronounced influence on the electronic states. The sensitivity to impurities suggests that this spin-singlet state may be a low-dimensional phenomenon. The EPR relaxation rate measurements show a spin-gap even in the doped system.

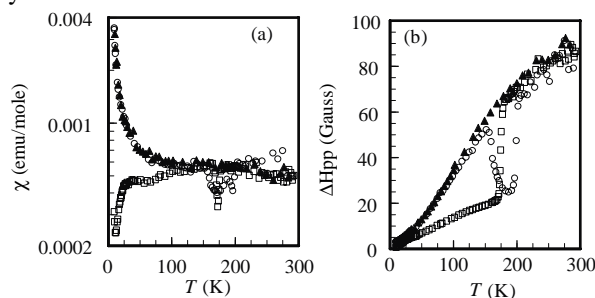


Figure 1. Temperature dependence of the (a) χ_{spin} , and (b) ΔH_{pp} along the a -axis (slow-cooling (open square), rapid-cooling (open circle) and the MT 5% doped salt (solid triangle)).

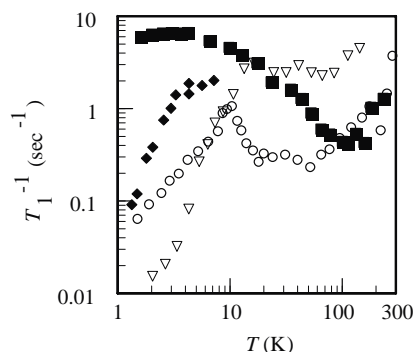


Figure 2. Temperature dependence of the NMR- T_1^{-1} under slow-cooling (^1H - T_1^{-1} (circle), ^{13}C - T_1^{-1} (triangle)) and rapid-cooling (^1H - T_1^{-1} (square), ^{13}C - T_1^{-1} (diamond)).

IV-C-2 Magnetic Properties of a New Two-Chain Organic Conductor: (CPDT-STF)-TCNQ

NAKAMURA, Toshikazu; TAKAHASHI, Toshihiro¹; TANIGUCHI, Masateru²; MISAKI, Yohji²; TANAKA, Kazuyoshi²
(¹Gakushuin Univ.; ²Kyoto Univ.)

[*Synth. Met.* **103**, 1900 (1999)]

(CPDT-STF)-TCNQ is a new organic conductor based on TCNQ and CPDT-STF where CPDT-STF is one of selenium-containing analogs of DT-TTF. Although the resistivity shows a metallic behavior down to 0.5 K, the spin susceptibility, χ_{spin} , is Curie-like at low temperatures. The purpose of the present study is to clarify the origin of the paramagnetic moments from microscopic points of view. Between 50 K and 300 K, the g -values gradually change with temperature. This indicates that the relative contributions to χ_{spin} of the CPDT-STF and TCNQ stacks are significantly temperature dependent. The decomposition of the χ_{spin} of (CPDT-STF)-TCNQ into the contributions of CPDT-STF, χ_{D} , and TCNQ, χ_{A} , was performed. The χ_{A} shows Curie-like behavior up to at least 200 K, indicating the existence of local moments on the TCNQ stacks. The spin concentration determined from the Curie constant is about 0.17 per formula unit assuming $S = 1/2$. On the other hand, the χ_{D} is almost temperature independent, suggesting a Pauli paramagnetism on the CPDT-TTF layers. It is quite natural that the metallic conduction is attributed to the itinerant electron on the CPDT-STF.

The nature of the local moments on TCNQ is now an open question. The spin concentration is different from the case of (BEDT-TTF)-TCNQ, where one spin per TCNQ dimer is localized. Experiments to address this problem are in progress.

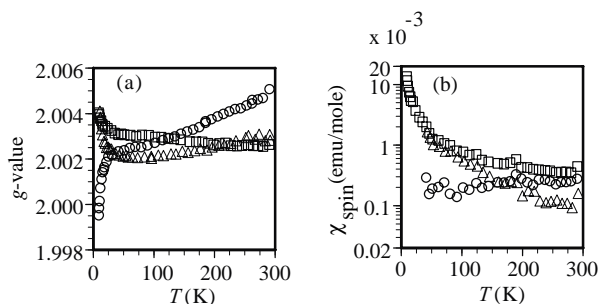


Figure 1. (a) Temperature dependence of the g -values ($//a^*$ (square), $//b^*$ (circle), $//c^*$ (triangle)). (b) Temperature dependence of the total χ_{spin} (square), and separate contributions of CPDT-STF (circle), TCNQ (triangle).

IV-C-3 ESR and NMR Investigation of β' - R_4Z [Pd(dmit) $_2$] $_2$

NAKAMURA, Toshikazu; TAKAHASHI, Toshihiro¹; AONUMA, Shuji²; KATO, Reizo²
(¹Gakushuin Univ.; ²ISSP, Tokyo Univ.)

[*Synth. Met.* **103**, 2142 (1999)]

β -type Pd(dmit) $_2$ salts and related salts show non-metallic behavior at ambient pressure. They undergo an antiferromagnetic transition, and that the paramagnetic states at ambient pressure should be considered as a Mott-Hubbard insulator. However, several problems remain unsolved; $^1\text{H-NMR}$ investigations showed the antiferromagnetic states possesses a small local magnetization. The local magnetizations and transition temperatures, T_N , are different between the Pd(dmit) $_2$ and the selenium-containing analogs Pd(dmise) $_2$ based salts. The main aim of this study is to clarify the antiferromagnetic states by systematic investigations of Pd(dmit) $_2$ salts. Figure 1 shows the temperature dependence of the EPR parameters of the Et $_2$ Me $_2$ P salts. The abrupt decrease of the χ_{spin} and the divergence of the ΔH_{pp} around 18 K obviously show the existence of the magnetic order. The observed g -tensor cannot be explained by that of single Pd(dmit) $_2$ molecule. We believe that this is due to the strong dimer structure of the Pd(dmit) $_2$ based organic conductors. The T_N and the amplitude of antiferromagnetic local moments determined by $^1\text{H-NMR}$ shows a close correlation with the cation size. The T_N seems to decrease as the inter-dimer interaction within stacks decreases. The Et $_2$ Me $_2$ -Sb salt, of which the inter-dimer interactions within stacks is comparable to those between stacks, shows no antiferromagnetic order down to 7 K. The detailed analysis is now going on.

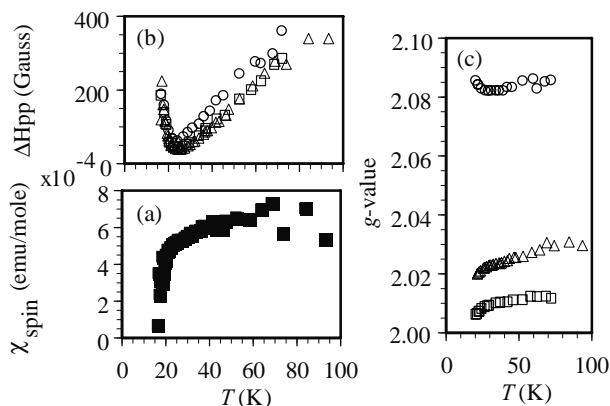


Figure 1. Temperature dependence of (a) the spin susceptibility, χ_{spin} , determined by EPR intensity, (b) the EPR linewidth, ΔH_{pp} , and (c) the g values ($//a^*$ (square), $//b^*$ (circle), $//c^*$ (triangle)).

IV-C-4 New Type Charge Localization in θ -(BEDT-TTF) $_2$ CsZn(SCN) $_4$

NAKAMURA, Toshikazu; MINAGAWA, Waka¹; KINAMI, Ryoji¹; TAKAHASHI, Toshihiro¹
(¹Gakushuin Univ.)

[*J. Phys. Soc. Jpn.* submitted]

$^1\text{H-NMR}$, EPR and static magnetic susceptibility measurements have been performed on an organic conductor, θ -(BEDT-TTF) $_2$ CsZn(SCN) $_4$. The $^1\text{H-NMR}$ - T_1^{-1} and the spin susceptibility exhibit anomalous enhancements at low temperatures. Around 20 K, where the spin susceptibility shows a minimum, the principal axes of the EPR g -tensor changed their directions, keeping the principal values constant. It indicates a possible change of the electronic nature. The low-temperature electronic state is discussed.

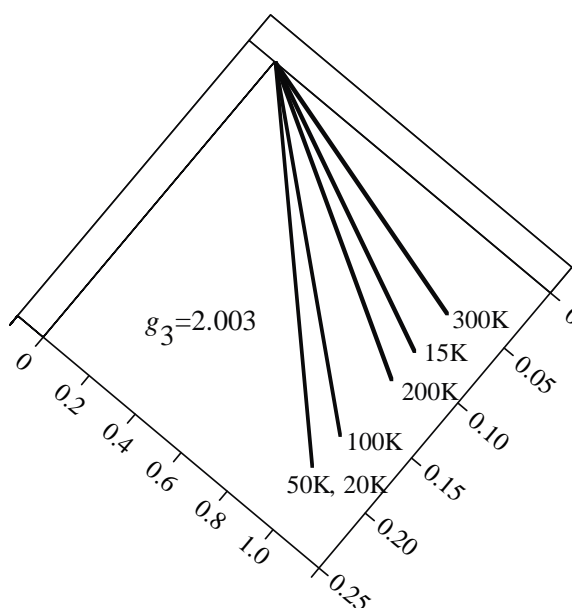


Figure 1. Temperature dependence of the direction of the principal axes of the g -tensor; magnified the scale for g_3 (top of view) at typical temperatures.

IV-D Thermodynamic Study of Organic Conductors

In order to get reliable information on the electron density of states and entropy distribution around various types of phase transitions, specific heat studies are inevitable. In this project, we aim at constructing several types of calorimeters available at low-temperatures and under magnetic fields and performing systematic investigation on organic materials from a thermodynamic viewpoint.

IV-D-1 Electronic Ground States of (BEDT-TTF)₂X System Studied by Specific Heat Measurements

NAKAZAWA, Yasuhiro; KANODA, Kazushi¹
(¹Univ. Tokyo)

[*Synrh. Met.* **103**, 1903 (1999)]

The 2:1 organic salts, (BEDT-TTF)₂X, give a variety of electronic phases such as metallic, superconductive, spin/charge density wave and antiferromagnetic insulating phases, etc. due to the variation of the molecular arrangement in the donor layers. The efforts to inquire into the origin and the peculiar features of the electronic structure of these phases have been widely made in these days, since they provide numerous interesting information of the condensed matter physics related to low-dimensional, low carriers and strongly correlated systems. Systematic studies to get an overall picture on the relationship between donor arrangement and the electronic ground states produced by π -electrons is now being performed from both experimental and theoretical viewpoints. In this study, we compare the low-temperature specific heat behavior of several 2:1 salts consist of BEDT-TTF molecules in order to get a systematic understanding of these π -electron systems from the thermodynamic viewpoint. Figures 1 and 2 show typical specific heat curves of metallic salts and Mott insulating salts, respectively. Although one can find finite γ term in the metallic samples, the Mott insulating salts does not have any electronic contribution in C_p/T vs T^2 curves at low-temperatures due to formation of charge-gap by the electron correlation effect.

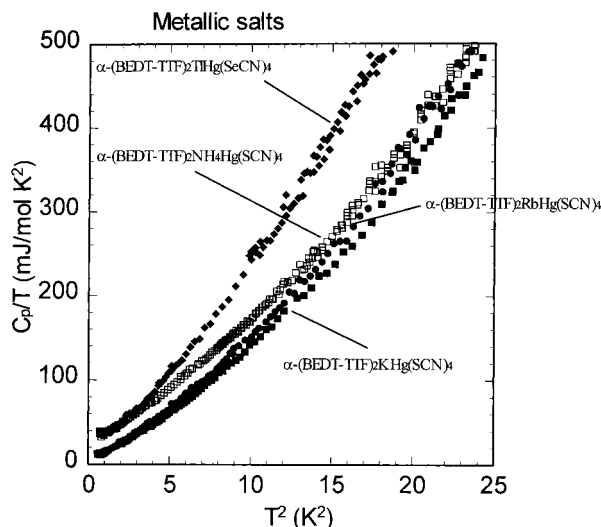


Figure 1. C_p/T vs T^2 plot of several metallic salts of (BEDT-TTF)₂X.

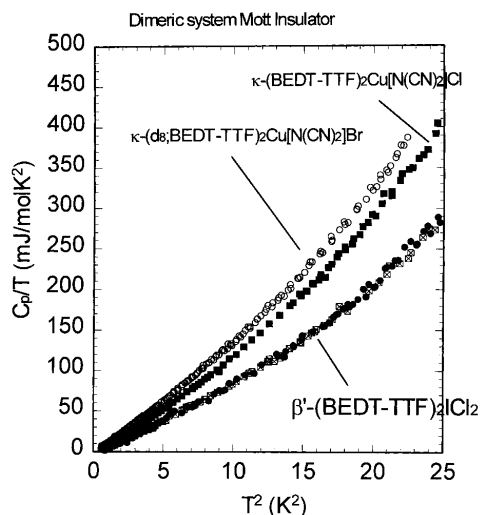


Figure 2. C_p/T vs T^2 plot of Mott insulating salts of (BEDT-TTF)₂X.

IV-D-2 Thermodynamic Investigation of the Electronic States of Deuterated κ -(BEDT-TTF)₂-Cu[N(CN)₂]Br

NAKAZAWA, Yasuhiro; KANODA, Kazushi¹
(¹Univ. Tokyo)

[*Phys. Rev. B* **60**, 4263 (1999)]

The low-temperature specific heat of the deuterated κ -(BEDT-TTF)₂Cu[N(CN)₂]Br situated in the critical region of the Mott transition in the κ -(BEDT-TTF)₂X systems was measured after different cooling processes, which are known to affect the superconducting volume fraction from the resistivity and the magnetic susceptibility measurements. Temperature and magnetic field dependences of the electronic specific heat do not show distinct variation by changing cooling rate from 0.07 K/min to 50 K/min and under magnetic field up to 6 T. We show in Figure 1 the low-temperature data obtained by a dilution refrigerator cooled down with the rates of 0.07 K/min, 0.8 K/min and 1.7 K/min from room temperature down to 4.2 K. The electronic specific heat coefficient, γ is found to be 0–1 mJ/molK² in all three curves and this values are much smaller than those of bulk superconducting materials of hydrogenated X = Cu[N(CN)₂]Br and Cu(NCS)₂.

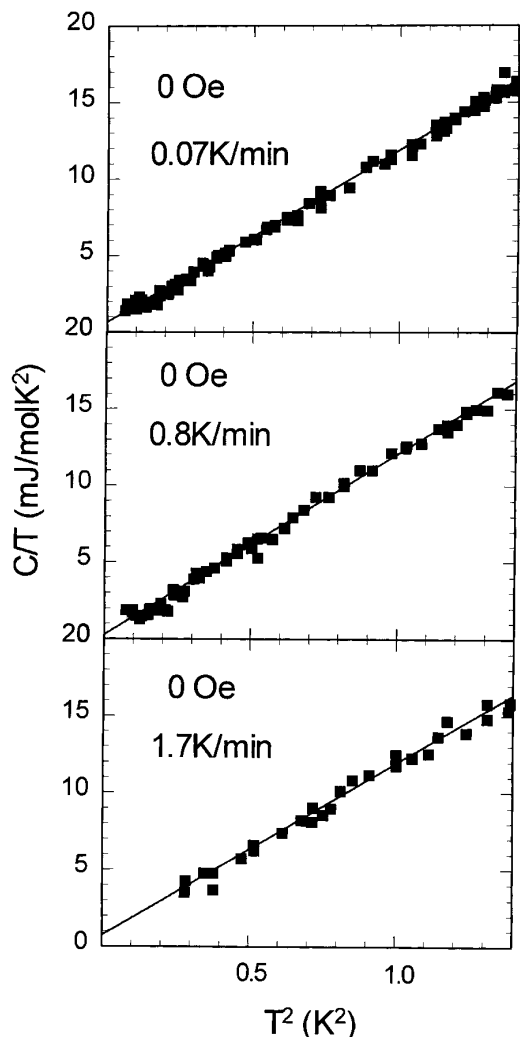


Figure 1. Low-temperature specific heat curves of κ -(d_8 ;BEDT-TTF) $_2$ Cu[N(CN) $_2$]Br cooled down at different rates of 0.07, 0.8, and 1.7 K/min.

IV-D-3 Electronic Specific Heat at the Boundary Region of Mott Transition in Two-Dimensional Electronic System of κ -(BEDT-TTF) $_2$ Cu[N(CN) $_2$]Br

NAKAZAWA, Yasuhiro; TANIGUCHI, Hiromi¹;
KAWAMOTO, Atsushi²; KANODA, Kazushi¹
(¹Univ. Tokyo; ²Hokkaido Univ.)

The electronic specific heat studies of partially deuterated single crystals of organic conductors κ -(BEDT-TTF) $_2$ Cu[N(CN) $_2$]Br which are situated across the critical boundary of band-width control type of Mott transition in two dimension are performed at low-temperatures below 3 K and under magnetic fields up to 10 T. In order to see the variation of normal-state electronic density of states near the transition, we had gradually access to the M-I boundary with the progressive dueteration of BEDT-TTF molecules and found that the electron density of states or effective mass in the metallic states diminishes towards the Mott boundary. This is in fine contrast to the case of V $_2$ O $_3$, where the Brinkmann and Rice's prediction of electron mass enhancement occurs in the critical region. This

result is marked a basis for the future study of electronic feature related to the unconventional superconductivity and also on the universality and variation of the Mott transition in two dimensional systems.

IV-E Photoelectron Spectroscopy of Organic Solids in Vacuum Ultraviolet Region

The works of ultraviolet photoelectron spectroscopy (UPS) with synchrotron radiation light source (UVSOR-UPS) of advanced organic materials have been proceeded to find their quantitative electronic structures and also to analyze their structures of assemblies.

IV-E-1 Angle-Resolved Photoemission Spectra of ω -(*n*-pyrrolyl) Alkanethiol Self-Assembled Monolayers: Possible Assemblies of Substituent Pyrrole

HASEGAWA, Shinji; YAKUSHI, Kyuya; INOKUCHI, Hiroo; OKUDAIRA, Koji K.¹; UENO, Nobuo¹; SEKI, Kazuhiko²; WILLICUT, J. Robert³; MACCARLEY, L. Robin³; MORIKAWA, Eizi⁴; SPRUNGER, T. Phillip⁴; SAILE, Volker⁴
(¹Chiba Univ.; ²Nagoya Univ.; ³Louisiana State Univ.; ⁴Louisiana State Univ. CAMD)

Angle resolved ultraviolet photoelectron spectra (ARUPS) on pyrrolyl-SAMs on polycrystalline Ag were measured by using synchrotron radiation. We found the π bands originated from the substituent pyrrole which are distinguishably observed from the bands of alkyl backbone. Since the π bands are available for the cue to probe the surface structures of pyrrole, we calculated the photoelectron angular distributions of them for the model structures obtained by molecular dynamics (MD) calculations. We revealed that two surface structures of pyrrole, face-stacked and herringbone structures, are possible for pyrrolyl-SAMs on Ag(111) and the herringbone structure is energetically favored.

The calculated photoelectron angular distributions can clearly distinguish between the face-stacked and herringbone structures of surface pyrrole, and give information on the orientation of pyrrole, the direction of pyrrolyl facing axis, and symmetry of the surrounding molecules. The ARUPS measurement for pyrrolyl-SAMs is promising for quantitative determinations of surface structures and now in progress.

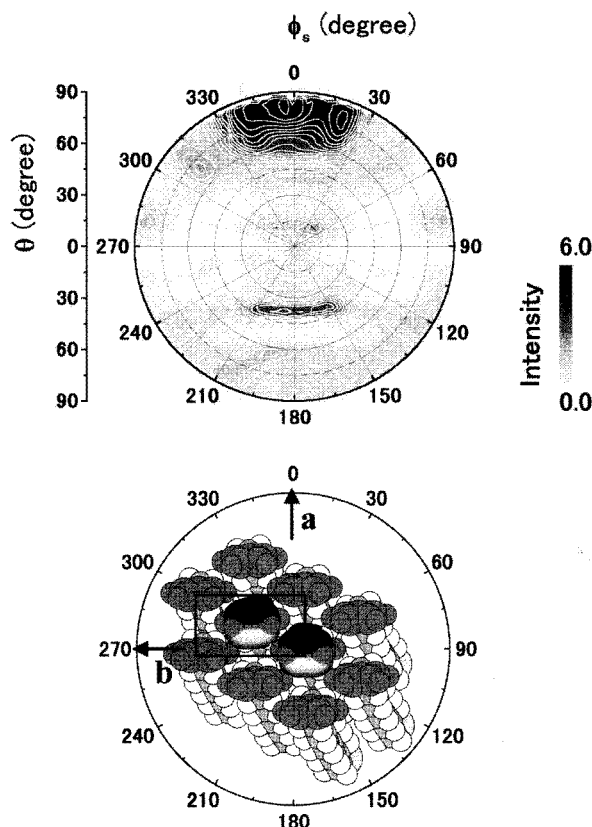


Figure 1. Calculated photoelectron angular distribution of π state within the single-scattering approximation. The photoelectron intensity is displayed by shading by the two-dimensional mapping with θ and ϕ_s . The illustration shows the face-stacked structure of pyrrolyl-SAMs obtained by MD calculation.

IV-E-2 Structure of Copper- and H₂-Phthalocyanine Thin Films on MoS₂ Studied by Angle-Resolved Ultraviolet Photoelectron Spectroscopy and Low Energy Electron Diffraction

OKUDAIRA, Koji K.¹; HASEGAWA, Shinji; ISHII, Hisao²; SEKI, Kazuhiko²; HARADA, Yoshiya¹; UENO, Nobuo
(¹Chiba Univ.; ²Nagoya Univ.)

[*J. Appl. Phys.* **85**, 6453 (1999)]

Angle-resolved ultraviolet photoelectron spectra (ARUPS) of copper phthalocyanine (CuPc) and metal-free phthalocyanine (H₂Pc) films (thickness from monolayer to 50–80 Å) on cleaved MoS₂ substrates were measured using monochromatic synchrotron radiation. Observed take-off angle (θ) and azimuthal angle (ϕ) dependencies of the top π band intensity were

analyzed quantitatively by the single-scattering approximation theory combined with molecular orbital calculations. The analysis indicated that the molecules lie flat on the MoS₂ surface in monolayer films of CuPc and H₂Pc. The azimuthal orientation of the molecules (angle between molecular axis and surface crystal axis of MoS₂), was found to be about -7° , -37° , or -67° for both monolayer films of CuPc and H₂Pc. In the azimuthal orientation, the analyses indicated that there are only molecules with counterclockwise rotation, although both clockwise and counterclockwise rotations are expected. From the low energy electron diffraction, the two-dimensional lattice structure of the monolayer film was obtained. On the basis of these two kinds of experimental results, the full structure of the monolayer film, the two-dimensional lattice and the molecular orientation at the lattice points, was determined. Furthermore, for the thick films it is found from the analyses of ARUPS that CuPc and H₂Pc molecules tilt about 10° from the surface plane.

IV-E-3 Electronic Structure of Poly (1,10-Phenanthroline-3,8-diyl) and Its K-doped State Studied by Photoelectron Spectroscopy

MIYAMAE, Takayuki; UENO, Nobuo; HASEGAWA, Shinji; SAITO, Yutaka¹; YAMAMOTO, Takakazu¹; SEKI, Kazuhiko²
(¹Tokyo Inst. Tech.; ²Nagoya Univ.)

[*J. Chem. Phys.* **110**, 2552 (1999)]

Ultraviolet photoelectron spectra were measured using synchrotron radiation for thin films of poly(1,10-

phenanthroline-3,8-diyl) (PPhen) and its potassium-doped state. Upon potassium doping of PPhen, two new states, which could be assigned to bipolaron bands, appear in the originally empty energy gap. The electronic structure of the neutral and potassium-doped states was theoretically analyzed using single-scattering approximation combined with semiempirical molecular orbital calculations.

IV-E-4 Electronic Structures of Alq₃/LiF/Al Interfaces Studied by UV Photoemission

YOSHIMURA, Daisuke; YOKOYAMA, Takahiro¹; ITO, Eisuke¹; ISHII, Hisao¹; OUCHI, Yukio¹; HASEGAWA, Shinji; SEKI, Kazuhiko¹
(¹Nagoya Univ.)

[*Synth. Met.* **102**, 1145 (1999)]

The electronic structure of tris (8-hydroxyquinolino) aluminum (Alq₃)/LiF/Al system was studied in relation to the enhancement of electron-injection efficiency by the insertion of LiF insulating layer at Alq₃/Al contact, using UV photoemission spectroscopy (UPS), X-ray photoelectron spectroscopy (XPS), and metastable atom electron spectroscopy (MAES). The observed energy separation between the HOMO of Alq₃ and the Fermi level of Al substrate increased from 2.7 eV to 3.0 eV by inserting 0.5 nm thick LiF layer. This result indicates that the LiF layer induces the decrease of the electron injection barrier. We also found extra states probably caused by the interaction at the Alq₃/Al interface. The spectral intensity of this extra state decreased with increasing LiF thickness, and vanished at 0.5 nm.

IV-F Electrical Conduction and its Related Properties of Organic Solid

To expand the research field of molecular conductors, we always consider to find a new category. One of them is three components organic semiconductors, conductors and superconductors. In this section, we present the works of three components organic superconductors based on C₆₀.

IV-F-1 Three Component Organic Superconductors: Intercalation of KH into C₆₀

IMAEDA, Kenichi; TIAN, Fuli; INOKUCHI, Hiroo; ICHIMURA, Kenji¹
(¹Kumamoto Univ.)

[*J. Solid State Chem.* **145**, 421 (1999)]

We have prepared (KH)₃C₆₀ as an initial composition by direct reaction of potassium hydride (KH) to C₆₀. (KH)₃C₆₀ had higher T_c (19.5 K) and larger lattice constant (14.351 Å), compared with K₃C₆₀ prepared by doping of potassium metal. The expanded lattice constant is suggestive of the intercalation of hydrogen. The evidence of the inclusion of hydrogen was given by mass-analyzed thermal desorption experiment. We have also prepared (NaH)_{4-x}(KH)_xC₆₀ to study the substitutional effect of KH to (NaH)₄C₆₀. It was found that the superconducting phase is stabilized by

substitution of only a few percent KH as seen in (NaH)_{3.9}(KH)_{0.1}C₆₀.

IV-F-2 Hydrogen Intercalation in Potassium-C₆₀

IMAEDA, Kenichi; INOKUCHI, Hiroo; ICHIMURA, Kenji¹; INOUE, Shin-ichi²; NAKAKITA, Satoshi²; OKAMOTO, Hiroshi²
(¹Kumamoto Univ.; ²Aichi Inst. Tech.)

[*Proceedings of ISIC10*]

Solid state ¹H NMR of (KH)₃C₆₀ was measured in the temperature range between -80 and 60°C . A doublet spectrum composed of main peak at -7.0 ppm and shoulder peak at ~ 0 ppm was observed at room temperature. The negative chemical shift of the main peak indicates that hydrogen in (KH)₃C₆₀ exists as a hydride-like ion. The 60°C spectrum became singlet at -5.8 ppm due to motional narrowing.

IV-G Magnetism and Superconductivity of BETS Conductors

Since the discovery of one-dimensional organic metals in early 1970s, a large progress has been made in the field of molecular conductors. The first discovery of organic superconductor (TMTSF)₂PF₆ was reported in 1980. We have found two new organic superconductors in 1986-87, one of which was the first κ -type organic superconductor, κ -(BEDT-TTF)₂I₃. The tremendous boom of copper oxide superconductor was started around the same time. Although many organic superconductors (especially κ -type organic superconductors based on BEDT-TTF) have been discovered since then, almost all people do not think that T_c of the hitherto-reported type of organic superconductor will become able to compete with the T_c of oxide superconductor. Therefore, it may be natural that the development of multifunctional conductors such as magneto-conducting systems attracts an increasing attention.

We have examined a series of BETS (= bis(ethylenedithio)tetraselenafulvalene) conductors with tetrahalide anions, MX₄ (M = Ga, Fe; X = Cl, Br). Our main interest is in the development of new types of conducting systems by incorporating Fe³⁺ magnetic ions in organic conductors having stable two-dimensional metal states. Two years ago, we have discovered an unprecedented superconductor-to-insulator transition in λ -type BETS conductors, λ -BETS₂Fe_{1-x}Ga_xCl₄ (0.35 < x < 0.5), where the interaction between localized magnetic moments of Fe³⁺ ions and π conduction electrons play an essential role. We have recently discovered the first antiferromagnetic organic metal exhibiting a superconducting transition.

IV-G-1 Chemical Control of Electrical Properties and Phase Diagram of a Series of λ -Type BETS Superconductors, λ -BETS₂GaBr_xCl_{4-x}

TANAKA, Hisashi¹; KOBAYASHI, Akiko¹; SATO, Akane; AKUTSU, Hiroki; KOBAYASHI, Hayao
(¹Univ. Tokyo)

[*J. Am. Chem. Soc.* **121**, 760 (1999)]

λ -BETS₂GaBr_xCl_{4-x} (0 < x < 2) is a molecular superconductor with strongly correlated conduction electrons. At ambient pressure, the superconducting transition could be observed for x < 0.75. The pressure and x dependencies of T_c were examined. The M-H curve at 2 K indicated the almost perfect Meissner state of the superconducting phase of λ -(BETS)₂GaCl₄ (M = magnetization; H = magnetic field). The magnetic susceptibility of λ -BETS₂GaBr_xCl_{4-x} increases with decreasing temperature down to about 60 K, below which the susceptibility becomes x-dependent and tends to be suppressed with increasing x. The isotropic decrease of the static susceptibility at lower temperature observed in the insulating system with x > 1.0 indicates the insulating ground state seems not to be antiferromagnetic but probably non-magnetic. The crystal structure determinations of a series of λ -BETS₂GaBr_xCl_{4-x} and the calculations of the intermolecular overlap integrals of the highest occupied molecular orbital of BETS were made to elucidate a key factor of the superconducting transition mechanism. The x dependence of intermolecular overlap integrals seems to suggest that the magnitude of the "spin gap" of the non-magnetic insulating state tends to be diminished with decreasing x.

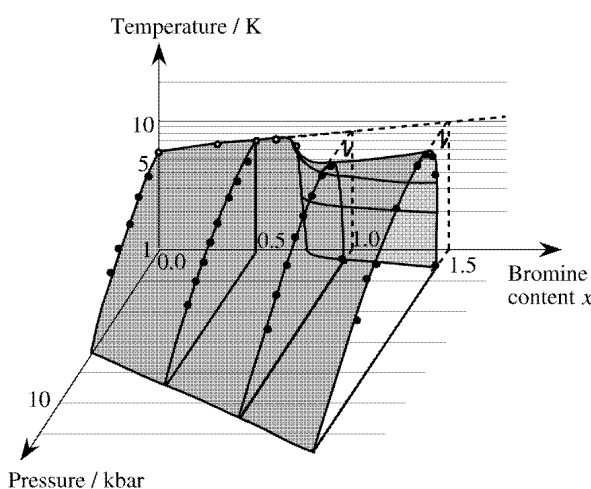


Figure 1. T - P - x phase diagram of λ -BETS₂GaBr_xCl_{4-x}. The region surrounded by shaded plane corresponds to the superconducting region.

IV-G-2 Evidence for the First Order Transition between High-temperature Superconducting and Low-temperature Insulating Phases in λ -BETS₂Fe_xGa_{1-x}Cl₄ (x ≈ 0.45)

TANAKA, Hisashi; KOBAYASHI, Hayao; KOBAYASHI, Akiko¹
(¹Univ. Tokyo)

We have recently discovered a novel superconductor-to-insulator transition in λ -BETS₂Fe_xGa_{1-x}Cl₄ (0.35 < x < 0.5). A sharp drop of the susceptibility at superconducting transition (T_c) and its recovery at lower temperature (T_{SC-I}) indicated that the crystal once transforms into superconducting state and then returns to the non-superconducting state with decreasing temperature. The large diamagnetic susceptibility at $T_{SC-I} < T < T_c$ observed by SQUID magnetometer showed conclusively the SC-I transition to be a bulk transition. In order to contribute to the better understanding of this unprecedented superconductor-to-insulator transition, we have carefully measured the temperature dependence of the resistivity on the freshly prepared crystal of λ -BETS₂Fe_xGa_{1-x}Cl₄ (x = 0.45). As

shown in Figure 1, the crystal showed the SC and SC-I transitions with decreasing temperature. In contrast to the sharp superconducting transition at 4.6 K, the SC-I transition showed a distinct hysteresis, showing the first-order nature of the SC-I transition.

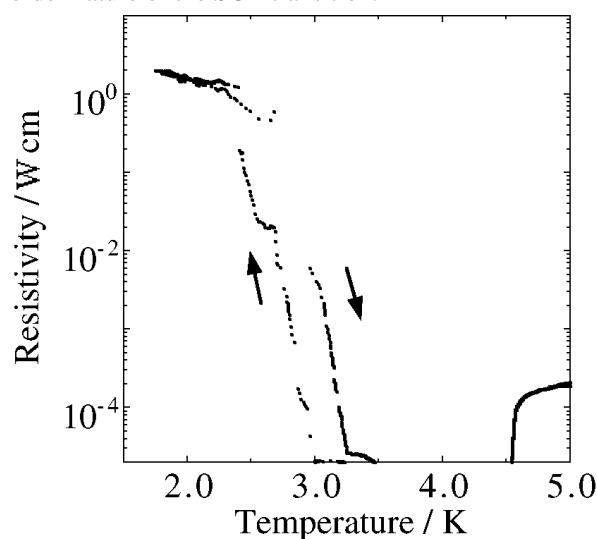


Figure 1. Resistivity behavior of λ -BETS₂Fe_xGa_{1-x}Cl₄ ($x = 0.45$).

IV-G-3 Coexistence of Antiferromagnetically Ordered Fe³⁺ Spins and Metal π -Electrons in λ -BETS₂FeCl₄

SATO, Akane; OJIMA, Emiko; KOBAYASHI, Hayao; HOSOKOSHI, Yuko; INOUE, Katsuya; KOBAYASHI, Akiko¹; CASSOUX, Patrick²
(¹Univ. Tokyo; ²CNRS)

[*Adv. Mater.* in press]

Recently we have studied the magnetic properties of λ -BETS₂FeCl₄ at high pressure. Since the 30 mg of the crystals was required for the high-pressure magnetic susceptibility measurements, the electrocrystallization experiments were repeated 25 times. The susceptibility was measured on SQUID magnetometer by using oriented thin needle crystals of λ -BETS₂FeCl₄ sealed in Teflon capsule and the Ti-Cu alloy high-pressure cell. The magnetic field was applied along the needle axes of the crystals (*//c*). At 2 kbar, sharp drop of magnetization suggesting strong π -d coupling was disappeared and only broad maximum was observed at low magnetic field. The broad maximum indicating the separation between π and d electron systems at high pressure became conspicuous with decreasing magnetic field. Only Fe³⁺ spins seems to be antiferromagnetically ordered at low temperature. Similar behavior was also observed at 3, 4 and 5 kbar. The *M-H* curve measured at 1 bar, 3 kbar and 5 kbar showed the spin flop behavior, consistent with the antiferromagnetic ordering of Fe³⁺ spins with easy axis along *c*. These facts indicate λ -BETS₂FeCl₄ to be the first organic conductor with the antiferromagnetic metal phase at high pressure.

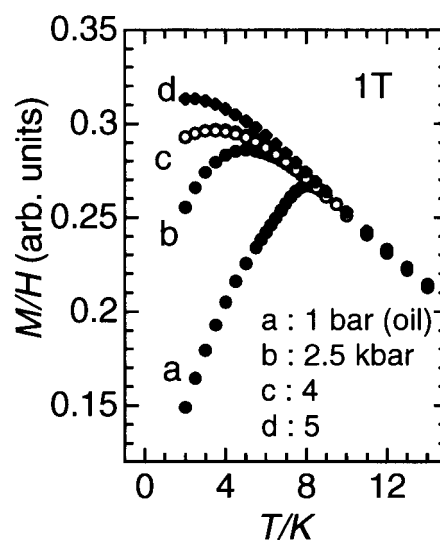


Figure 1. Temperature dependence of the susceptibility of λ -BETS₂FeCl₄ at high pressure.

IV-G-4 Pressure-Induced Superconducting Transition of λ -(BETS)₂FeCl₄ with π -d Coupled Antiferromagnetic Insulating Ground State at Ambient Pressure

TANAKA, Hisashi; ADACHI, Takafumi¹; OJIMA, Emiko; FUJIWARA, Hideki; KOBAYASHI, Hayao; KOBAYASHI, Akiko²; CASSOUX, Patrick³
(¹IMS and Electrotech. Lab.; ²Univ. Tokyo; ³CNRS)

[*J. Am. Chem. Soc.* in press]

The resistivities of λ -(BETS)₂FeCl₄ were measured at high pressure down to 0.5 K. The characteristic π -d coupled antiferromagnetic insulating ground state was destabilized under pressure and the superconducting transition was observed above 3 kbar. Since the Fe³⁺ spins has been reported to be antiferromagnetically ordered at the temperature region above the superconducting phase, the present results suggest that λ -(BETS)₂FeCl₄ undergoes a transition from antiferromagnetic metal phase to superconducting phase at high pressure. T_c was decreased with increasing pressure: the value of dT_c/dP (-0.5 deg/kbar) is almost equal to that of λ -(BETS)₂GaCl₄. The field-restored highly conducting state (FRHCS) was observed at 2.5 kbar. The critical magnetic field of FRHCS (55 kOe) was almost a half of that at ambient pressure (110 kOe). When the magnetic field was applied perpendicular to the *ac* plane (conduction plane) at 3.5 kbar and 0.55 K, the superconducting state was broken at 5–8 kOe. While, for the field parallel to the *ac* plane, the resistivity began to appear at 0.5 kOe and increased up to 13 kOe.

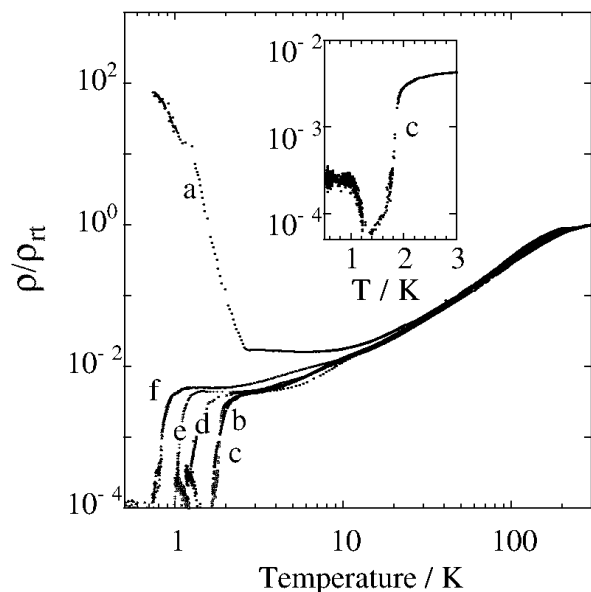


Figure 1. The resistivity of λ -(BETS) $_2$ FeCl $_4$ at 2.5 (a), 3.0 (b), 3.2 (c), 4.0 (d), 4.5 (e) and 5.0 (f) kbar. The inset shows the anomalous resistivity behavior observed at 3.2 kbar.

IV-G-5 Electric and Magnetic Properties of BETS Conductor with Modified λ -type Structure, λ' -BETS $_2$ GaBr $_4$

TANAKA, Hisashi¹; KOBAYASHI, Akiko¹; KOBAYASHI, Hayao
(¹Univ. Tokyo)

[Chem. Lett. 133 (1999)]

We have studied a series of BETS conductors with mixed-halogen gallate anions, GaBr $_x$ Cl $_{4-x}$ ⁻. The anion sites of the λ -type salt cannot accommodate large anions. Then the structure is modified into " λ' -structure" for $x > 2.0$. The physical properties of λ' -(BETS) $_2$ GaBr $_4$ are quite different from those of λ -(BETS) $_2$ GaBr $_x$ Cl $_{4-x}$. The resistivity was almost temperature independent down to 50 K below which it increased gradually. Above ca. 3 kbar, the metallic state was stabilized, but the superconducting behavior could not be found down to 2 K. Extended-Hückel tight-binding band calculation and temperature dependencies of resistivity and magnetic susceptibility of λ' -(BETS) $_2$ -GaBr $_4$ suggest the semimetal-to-insulator transition around 50 K. Thus despite of the apparent structural similarity of the λ - and λ' -salts, the electronic state of these two systems are completely different.

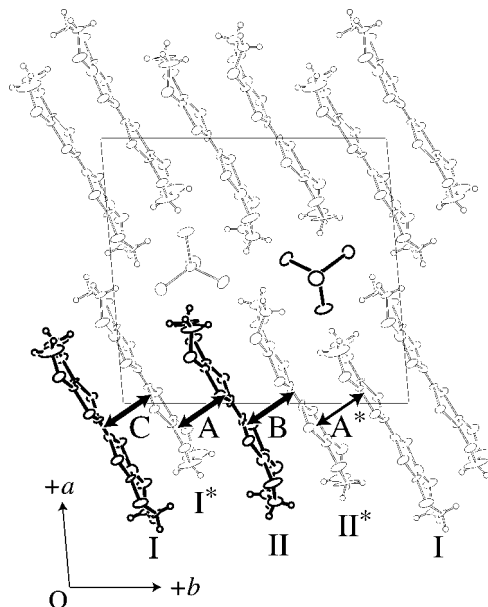


Figure 1. Crystal structure of λ' -BETS $_2$ GaBr $_4$ viewed along the c axis.

IV-G-6 Antiferromagnetic Organic Metal Exhibiting Superconducting Transition, κ -(BETS) $_2$ FeBr $_4$

OJIMA, Emiko; FUJIWARA, Hideki; KATO, Kiyonori; KOBAYASHI, Hayao; TANAKA, Hisashi¹; KOBAYASHI, Akiko¹; TOKUMOTO, Madoka²; CASSOUX, Patrick³
(¹Univ. Tokyo; ²Electrotech. Lab.; ³CNRS)

[J. Am. Chem. Soc. **121**, 5581 (1999)]

The electric and magnetic properties of κ -(BETS) $_2$ -FeBr $_4$ show this system to be the first ambient-pressure antiferromagnetic organic metal ($T_N = 2.5$ K). The characteristic field dependence of the magnetization at 2 K indicates a helical spin structure. When the magnetic field is applied to the conduction plane (\parallel crystal plane), the magnetization increases very rapidly and tends to be saturated above 20 kOe. While the magnetization increases almost linearly up to about 70 kOe for the field perpendicular to the crystal plane. A small resistivity drop observed at T_N gives a clear evidence for the existence of the interaction between π metal electrons and localized magnetic moments. Furthermore, this system undergoes a superconducting transition at 1.0 K.

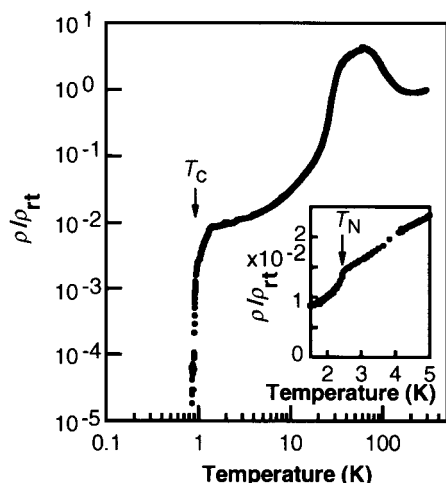


Figure 1. Resistivity of κ -(BETS)₂FeBr₄ at 0.5-300 K measured along the *ac* plane.

IV-G-7 A New κ -Type Organic Superconductor Based on BETS Molecules, κ -(BETS)₂GaBr₄

TANAKA, Hisashi; OJIMA, Emiko; FUJIWARA, Hideki; NAKAZAWA, Yasuhiro; KOBAYASHI, Hayao; KOBAYASHI, Akiko¹
(¹Univ. Tokyo)

We have recently reported that κ -(BETS)₂FeBr₄ undergoes successive phase transitions with lowering temperature from paramagnetic metal state to antiferromagnetic metal state at 2.5 K (*T_N*) and from antiferromagnetic metal state to superconducting state at 1.0 K (*T_c*). Furthermore, it is highly possible that κ -(BETS)₂-

FeBr₄ is the first antiferromagnetic organic superconductor, which was one of the final targets of the studies on the development of new organic conductors. Since the resistivity behavior of κ -(BETS)₂GaBr₄ has been reported to resemble to that of κ -(BETS)₂FeBr₄, a superconducting transition will be expected also in κ -(BETS)₂GaBr₄. In fact, we have found the superconducting transition of κ -(BETS)₂GaBr₄ around 0.5-1.0 K. This finding indicates *T_c* of κ -(BETS)₂MBr₄ (M = Fe, Ga) to be almost independent of the existence of magnetic anions. A way to develop novel organic superconductors with controlled antiferromagnetic interactions is suggested.

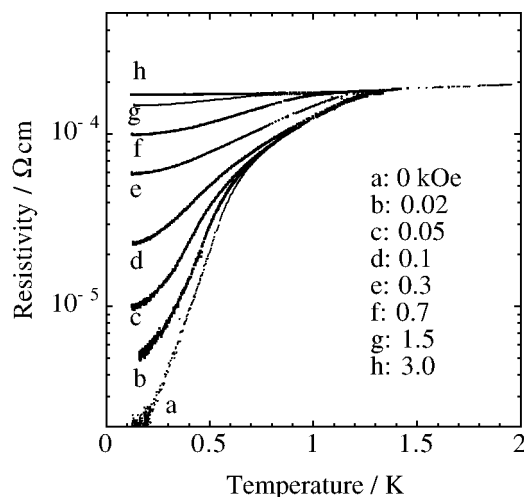


Figure 1. The magnetic field-dependence of the resistivities of κ -(BETS)₂GaBr₄ at 0-3.0 kOe.

IV-H Structural and Electrical Properties of Molecular Crystals at Low Temperature and/or High Pressure

Since the molecular crystal is very soft and rich in the structural freedom, various structural phase transitions will be expected at high pressure and/or low temperature. Moreover, the electronic properties of molecular crystal are very sensitive to the structure change. Therefore the precise three-dimensional X-ray structure analyses at high pressure and/or low temperature are important in the studies on solid state properties of molecular crystals. More than several years ago we have developed a simple X-ray imaging plate system equipped with low-temperature refrigerator, which made the low-temperature X-ray study very easy. At present, we are trying the high-pressure (or high-pressure and low-temperature) X-ray experiments by using specially designed diamond anvil cell and X-ray imaging plate system.

Usually, the high-pressure resistivity measurements of molecular conductors have been made by using clamp type pressure cell, which enables us to measure the resistivities up to about 20 kbar. For the studies on the solid state properties of molecular solid at high pressure, it is highly desired to find a way to perform the resistivity measurements by using diamond anvil cell. We have recently succeeded to measure the resistivity of thin needle crystals of organic materials up to 100 kbar.

IV-H-1 Low Temperature Structure Analysis of Unannealed TDAE**C*₆₀ Single Crystal

NARYMBETOV, Bakhyt¹; KOBAYASHI, Hayao; TOKUMOTO, Madoka²; OMERZU, Ales³; MIHAILOVIC, Gragan³
(¹IMS and Uzbek Acad. Sci.; ²Electrotech. Lab.; ³Jozef Stefan Inst., Slovenia)

[*Chem. Commun.* 1511 (1999)]

Since the discovery of the ferromagnetism in TDAE**C*₆₀ compound (TDAE = tetrakis(di-methyl-amino)ethylene) with the *T_c* = 16 K it has been intensively studied by various experimental methods. However, till now a detailed crystal structure based on single crystal diffraction data has not been determined because in this materials the *C*₆₀ molecules have

orientational disorder at room temperatures. We have carried out an X-ray diffraction study of an unannealed TDAE* C_{60} single crystal at low temperatures down to 7 K which have allowed access to detailed structural characteristics of the compound (freshly grown, unannealed crystal of TDAE* C_{60} doesn't show the ferromagnetic properties but they become ferromagnet after annealing the crystal at 20–100 °C). The structure was solved and refined based on the space group $C2/c$ for the set of data obtained at 7 and 11 K. There are four chemically equivalent C_{60} · $C_2(NC_2H_6)_4$ units per unit cell. The packing of the unit cell shows that C_{60} anions are located at inversion centers and form a chain along the c -axis with the shortest distance between molecular centers equal to 9.915 Å at that temperatures. The obtained configurations of TDAE are in reasonable agreement with predictions, which testifies to a charge state of TDAE of +1.

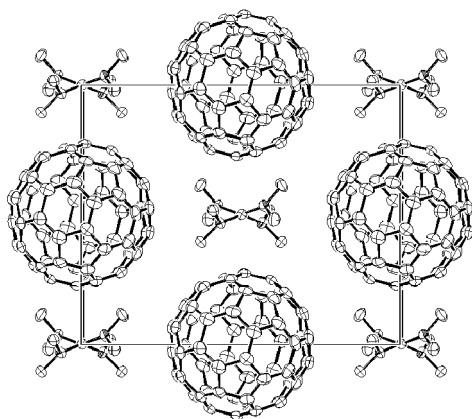


Figure 1. The projections of the C_{60} *TDAE crystal structure along the c -axis.

IV-H-2 X-Ray Diffraction Study of a TDAE* C_{60} Single Crystal

NARYMBETOV, Bakhyt¹; KOBAYASHI, Hayao; TOKUMOTO, Madoka²; OMERZU, Ales³; MIHAJLOVIC, Gragan³
(¹IMS and Uzbek Acad. Sci.; ²Electrotech. Lab; ³Jozef Stefan Inst., Slovenia)

Despite extensive efforts of researchers, there still remain questions about the origin and the nature of low temperature ground state of a TDAE* C_{60} compound. It has been suggested that there is a rotational randomness of C_{60} molecules in TDAE* C_{60} crystals and that the magnetism could strongly depend on the merohedral degree of freedom. The freshly grown single crystals are found to be ordered antiferromagnetically and annealing in temperature range 20–100 °C results in an enhanced ferromagnetic ordering of the samples. We have performed X-ray diffraction studies of TDAE* C_{60} single crystal in temperature range 270–7 K before and after annealing the crystal at 70 °C as well as its structure characterization at temperatures 160, 30, 11 and 7 K for unannealed sample and at low temperatures (below 16 K) for annealed sample. These studies show that for both unannealed and annealed TDAE* C_{60} single crystal at low temperatures there are structure transformations below 50 K. Remarkable changes of X-

ray diffraction patterns occur below 50 K and a characteristic feature of it is an appearance of diffuse lines. Observed appearance of diffuse lines on diffraction patterns below 50 K confirms the presence of ordering process, which proceeds several hours. Low temperature state of unannealed crystal is characterized by disappearing of the diffuse lines after keeping the crystal at temperatures below 50 K for about 3–4 hours. Distinctive feature in the case of annealed TDAE* C_{60} crystal is that below 50 K with the time the diffuse lines are transformed in an additional diffraction spots. X-ray oscillation patterns show that the positions of additional spots coincide with those for a primitive unit cell, which testify to a tendency of the crystal lattice to transformation from C-centered type to primitive one.

IV-H-3 Structure Transformation of a C_{60} * Na_x (THF)_y below 70 K

NARYMBETOV, Bakhyt¹; OJIMA, Emiko; OGATA, Hironori; KOBAYASHI, Hayao; KOBAYASHI, Akiko²; MORIYAMA, Hiroshi³
(¹IMS and Uzbek Acad. Sci.; ²Univ. Tokyo; ³Toho Univ.)

$Na_x(THF)_yC_{60}$ is the first metallic single crystal C_{60} compound grown by an electrocrystallization process. The studies of conductivity and magnetic properties of the crystals have revealed presence of metal-metal transition at 175 K and another phase transition at around 50 K. It has been found that the crystals have a hexagonal unit cell and the presence of phase transition around 170 K has been confirmed by X-ray diffraction experiments earlier. We have carried out low temperature X-Ray diffraction studies of $Na_x(THF)_yC_{60}$ by using the IP system equipped with liquid helium cooling device. The obtained diffraction patterns testify that there is a structure transformation of the crystal below 70 K which is shown as increase of the unit cell volume three times. Observed reflections on the diffraction patterns at low temperatures are indexed in hexagonal unit cell and the lattice parameters at 15 K are: $a = 26.207(12)$, $c = 9.868(3)$ Å, $V = 5869(8)$ Å³. Analysis of the collected intensity array shows that the space group is $P-3c1$ (or $P-3$) with the six molecules of C_{60} per unit cell, one independent position for C_{60} molecule and two positions for $Na_x(THF)_y$ with partial population of the equivalent positions. It seems that even at low temperatures fullerene molecules have a strong orientational disorder as well as a strong disorder of $Na_x(THF)_y$ on the symmetrically equivalent positions.

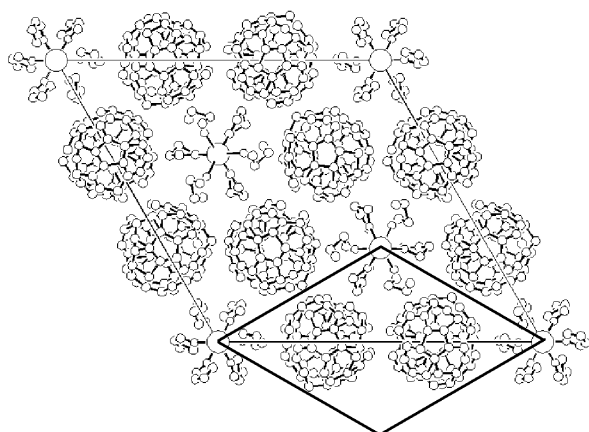


Figure 1. Schematic presentation of $C_{60}Na_x(THF)_y$ unit cell below 50 K. Unit cell at room temperature is shown by bold lines.

IV-H-4 High Pressure Structure of $[(C_2H_5)_2(CH_3)_2N][Pd(dmit)_2]_2$

ADACHI, Takafumi¹; NARYMBETOV, Bakhyt²; KOBAYASHI, Hayao; KOBAYASHI, Akiko³
(¹IMS and Electrotech. Lab.; ²IMS and Uzbek Acad. Sci.; ³Univ. Tokyo)

With the aim of setting up the high pressure (or high-pressure and low-temperature) single crystal X-ray apparatus by using diamond anvil cell, we are examining the crystal structure of a high-pressure superconductor, $[(CH_3)_2(C_2H_5)_2N][Pd(dmit)_2]_2$ ($T_c = 4$ K at 2.4 kbar). Several years ago, we have proposed a HOMO-LUMO inversion mechanism to explain an anomalous P - T phase diagram of $[(CH_3)_2(C_2H_5)_2N][Pd(dmit)_2]_2$ where the insulating phase appears at higher pressure region above the superconducting phase. We have analyzed the structure up to 10 kbar by using specially designed diamond anvil cell without Be-supporting disks. The diffraction spots were detected by X-ray imaging plate. In order to obtain the information on the high-pressure structure at low-temperature, we are trying the high-pressure X-ray experiments by using low-temperature imaging plate system.

IV-H-5 High-Pressure Four-Probe Resistivity Measurements of the Soft Organic Single Crystals up to 100 kbar

ADACHI, Takafumi¹; KOBAYASHI, Hayao; MIYAZAKI, Takafumi²; TOKUMOTO, Madoka³
(¹IMS and Electrotech. Lab.; ²Ehime Univ.; ³Electrotech. Lab.)

Recently, the electric properties of solids at extremely high pressure has attracted much attention. The superconductivity of oxygen discovered around 1 Mbar by using diamond anvil cell may be one of the best examples. On the other hand, the pressure of the usual clamp-type high pressure cell used for the single crystal experiments on the organic compounds cannot exceed *ca.* 25 kbar. In order to obtain the sufficiently accurate resistivity data above 100 kbar, an improvement of diamond anvils technique seems to be

inevitable. Since the report by Mao and Bell who measured the resistivity of string-shaped metal sample by using MgO gasket and pressure medium of soft powder (*e.g.* NaCl), the four-probe high-pressure resistivity measurements were made by diamond anvil cell. In order to apply high-pressure resistivity technique to soft organic crystals, the requirements for good Ohmic contacts and quasi-hydrostatic pressure will be essential. We have recently established an improved method applicable for the single crystal resistivity measurements up to 100 kbar.

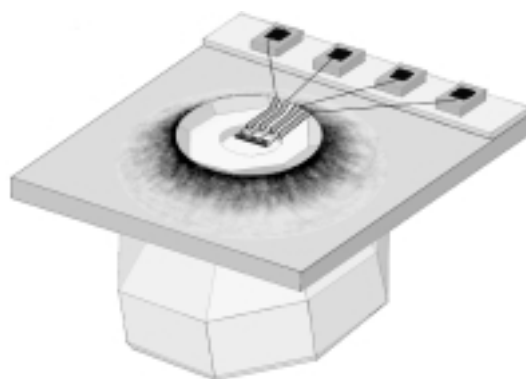


Figure 1. An illustration of the setup of diamond anvil four-probe resistivity cell.

IV-H-6 Resistivity Behavior of Organic Conductor, $\beta'-(BEDT-TTF)_2ICl_2$ up to 100 kbar

ADACHI, Takafumi¹; KOBAYASHI, Hayao; MIYAZAKI, Takafumi²; TOKUMOTO, Madoka³
(¹IMS and Electrotech. Lab.; ²Ehime Univ.; ³Electrotech. Lab.)

$\beta-(BEDT-TTF)_2I_3$ is one of the well-known organic superconductors discovered in 1984. An analogous conductor with smaller anions and modified β -type structure, $\beta'-(BEDT-TTF)_2ICl_2$ has an antiferromagnetic insulating ground state at ambient pressure. We have tried to check the possibility of the superconducting transition at high pressure by adopting the diamond anvil four-probe resistivity technique. The resistivities were successfully measured up to 100 kbar. To our knowledge, this is the first four-probe resistivity measurements on single organic crystal around 100 kbar. The activation energy was decreased with increasing pressure and metallic state appeared around 80 kbar. The room-temperature resistivity was $10^{-2} \Omega$ cm around 80 kbar, which was about three orders of magnitude smaller than that at ambient pressure (20Ω cm). However, the superconducting phase could not be found. Unexpectedly, around 100 kbar, the resistivity was gradually increased with the time, indicating a pressure-induced solid state reaction.

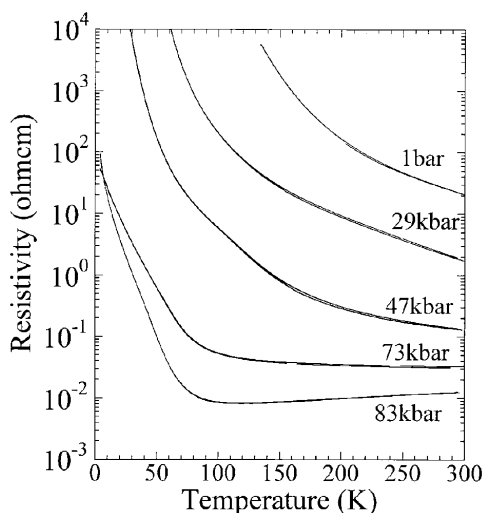


Figure 1. Resistivities of β' -(BEDT-TTF) $_2$ ICl $_2$ up to 80 kbar.

IV-I Development of New Molecular Conductors

The development of new materials is the most important driving force for the field of solid state chemistry. The recent progress in the concept of the molecular design enriched greatly the physics and chemistry of crystalline molecular solids. The appearance of various types of molecular metals, superconductors and molecular ferromagnets have attracted an increasing interest of chemists and physicists. We must grow out of the conventional design of molecular conductors for the future development. In these points of view we have performed the development of several types of new molecular components for organic molecular conductors. In the study of ditellurium bridged polyacene donors and propyleneditelluro substituted TTF, we have determined the whole of the crystal structures and physical properties. We are now examining new guiding principles for designing the organic conductors. Furthermore we have developed the novel organic donor containing a stable organic radical part to investigate the interaction between itinerant electrons of the charge-transfer complexes and localized spins of the organic stable radical parts for the development of novel organic conducting-magnetic hybrid materials.

IV-I-1 New Stable Metallic Salt Based on a Donor Molecule Containing *peri*-Ditellurium Bridges, TMTTeN(SCN) $_{0.88}$

OJIMA, Emiko; NARYMBETOV, Bakhyt; FUJIWARA, Hideki; KOBAYASHI, Hayao; KOBAYASHI, Akiko¹; TAKIMIYA, Kazuo²; OTSUBO, Tetsuo²; OGURA, Fumio³
(¹Univ. Tokyo; ²Hiroshima Univ.; ³Kinki Univ.)

[Chem. Lett. 845 (1999)]

Recently we have discovered the TMTTeN salts with Ag(CN) $_2^-$ and Au(CN) $_2^-$ anions showing metallic behavior down to 50 K. They have tetragonal structures and quasi three-dimensional Fermi surfaces. Recently, we have found a new stable metallic salt, TMTTeN(SCN) $_{0.88}$. The crystal structure is not isostructural to the structures of the Ag(CN) $_2^-$ and Au(CN) $_2^-$ salts. That is, penetration of the SCN $^-$ anion into the TMTTeN lattice leads to a modification of the packing of the TMTTeN molecules along the *c*-axis of the crystals. As shown in Figure 1, there are many intermolecular Te...Te contacts less than the sum of the van der Waals radii (4.2 Å) and three-dimensional network through the tellurium atoms is developed. The salt shows very high room-temperature conductivities (400–600 S cm $^{-1}$) and stable metallic behavior down to low temperature (4.2 K). The paramagnetic susceptibility of TMTTeN(SCN) $_{0.88}$ is almost constant throughout the

temperature range, indicating Pauli paramagnetism of the system [1.6 – 1.9×10^{-4} emu mol $^{-1}$]. Thus, the salt is considered to keep stable metallic nature down to liquid helium temperature.

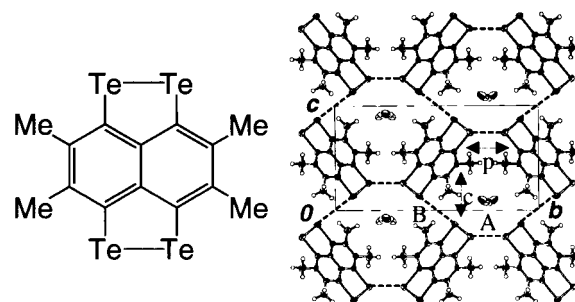


Figure 1. Structure of TMTTeN and crystal structure of TMTTeN(SCN) $_{0.88}$.

IV-I-2 Synthesis, Structures and Properties of New Organic Conductors Based on Tellurocycle-Fused TTF Donor Molecules

OJIMA, Emiko; FUJIWARA, Hideki; KOBAYASHI, Hayao; KOBAYASHI, Akiko¹
(¹Univ. Tokyo)

[Adv. Mater. in press]

In the search for excellent electron donors compos-

ing organic conductors, the concern for the tellurium-containing tetrathiafulvalene (TTF) derivatives has been growing for the last several years because a new metallic system with wide bandwidth and high dimensionality is expected to appear due to the large electron cloud of tellurium atoms. In addition, the conducting salts based on tellurium-containing donor molecules are interesting because the tellurium network is dominant for the construction of whole the crystal structure. Therefore we focused on the tellurocycle-fused TTF donor molecules. In this communication we reported the synthesis, crystal structure and electrochemical property of a new tellurocycle-fused TTF donor, 4,5-dimethyl-4',5'-propyleneditelluro-TTF **1**. We clarified the DA type crystal structure of the TCNQ complex of **1**. Furthermore, we prepared the several cation radical salts by use of the donor **1** and cleared that the unsymmetrical donor **1** are subject to the transformation to the dimerized donor **2** during the electrochemical oxidation. Although the obtained conducting salts are all semiconductors, those tellurium-containing donors have very interesting and unique molecular and crystal structures.

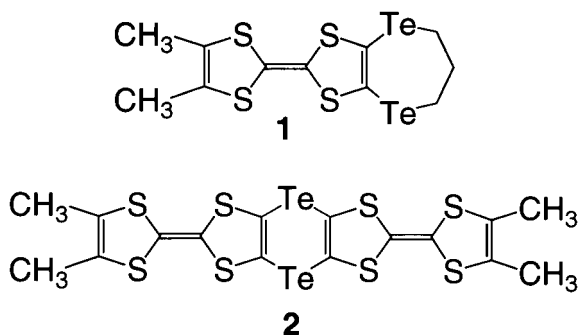


Figure 1. Structures of **1** and **2**.

IV-I-3 New π -Extended Organic Donor Containing a Stable TEMPO Radical as a Candidate for Conducting-Magnetic Multifunctional Materials

FUJIWARA, Hideki; KOBAYASHI, Hayao

[*Chem. Commun.* in press]

Recent studies on the molecular conductors and superconductors containing magnetic transition metal anions, such as the $(\text{ET})_2[(\text{H}_2\text{O})\text{Fe}(\text{C}_2\text{O}_4)_3] \cdot \text{C}_6\text{H}_5\text{CN}$ salt, a series of λ -(BETS) $_2\text{Fe}_x\text{Ga}_{1-x}\text{Cl}_4$ alloy salts and κ -(BETS) $_2\text{FeBr}_4$ salt, have stimulated the interest for the investigation of the interplay between the conductivity and magnetism in the research for new organic conductors. From the view point of realization of metallic conductivity, we supposed a molecular design as a fusion of a stable TEMPO radical part to the DTET-TTF [methylidene-1,3-dithiolo[4,5-*d*]-4,5-ethylenedithio-TTF] skeleton, which is a promising building block for realizing stable metallic behavior down to low temperature, such as the cases of MeDTET and CPDTET salts. We have examined the structure and physical properties of the $\text{Au}(\text{CN})_2^-$ salt of TEMPOET. The $\text{Au}(\text{CN})_2^-$ salt was electrochemically prepared. X-

Ray crystallographic analysis revealed that the D:A ratio of this salt is 2:3 and the TEMPOET donors form sheet-like structures. There is short O...O contacts (3.24(2) Å) between donor sheets. The room temperature electrical conductivities is low value of $10^{-3} \text{ S cm}^{-1}$ due to the highly oxidized state and undesirable stacking of donors. The small room temperature magnetic susceptibility ($9.6 \times 10^{-4} \text{ emu mol}^{-1}$ for 2:3 salt) suggests the existence of intramolecular spin singlet formation and/or intermolecular strong antiferromagnetic spin configuration.

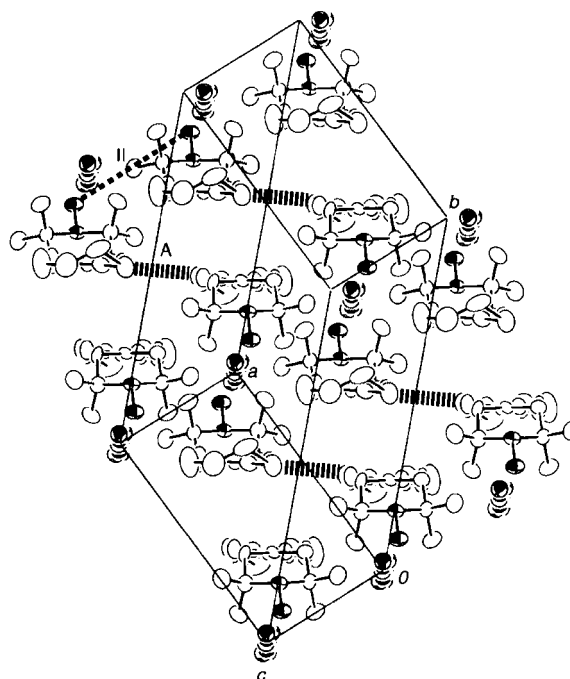


Figure 1. Crystal structure of $(\text{TEMPOET})_2[\text{Au}(\text{CN})_2]_3$.

IV-I-4 Synthesis and Properties of New Organic Donor Containing Two Stable TEMPO Radical Parts

FUJIWARA, Hideki; KOBAYASHI, Hayao

Organic molecular magnetism has become very active field of research for the material chemistry and physics since the discovery of the first pure organic ferromagnet in *p*-nitrophenyl nitronyl nitroxide (β -NPNN) in 1991 and successive development of several ferromagnets based on aminoxyl radicals such as 2,2,6,6-tetramethylpiperidinyloxy (TEMPO) and 4,4,5,5-tetramethyl-2-imidazoline-1-oxyl-3-oxide (NN) radicals. On the other hand, recent studies on the molecular conductors and superconductors containing magnetic transition metal anions have stimulated the interest for the investigation of the interplay between the conductivity and magnetism in the research for new organic conductors. Recently we have synthesized a donor molecule containing a stable TEMPO radical part and reported its electrochemical and magnetic properties. Furthermore we have prepared several cation radical salts and investigated their conducting and magnetic properties. In this context, further development of such stable radical-containing donor molecules

is of interest. In this work, we synthesized a new donor molecule containing two TEMPO radical parts **1** and investigated its ESR spectra and magnetic susceptibility.

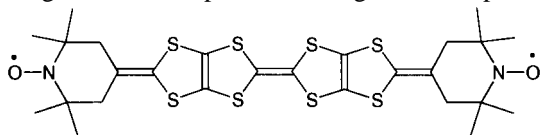


Figure 1. Structure of **1**.

IV-I-5 Origin of the High Electrical Conductivity of Neutral $[\text{Ni}(\text{ptdt})_2]$ — A Route to Neutral Molecular Metal

KOBAYASHI, Akiko¹; TANAKA, Hisashi¹; KUMASAKI, Mieko¹; TORII, Hajime¹; NARYMBETOV, Bakhyt²; ADACHI, Takafumi³
(¹Univ. Tokyo; ²IMS and Uzbek Acad. Sci.; ³IMS and Electrotech. Lab.)

[*J. Am. Chem. Soc.* in press]

A novel neutral nickel complex molecule with the extended TTF dithiolato ligand, propylenedithiotetrathiafulvalenedithiolate [$\text{ptdt}^{2-} = (\text{S}_8\text{C}_9\text{H}_6)^{2-}$], was synthesized. In the $[\text{Ni}(\text{ptdt})_2]$ crystal, $[\text{Ni}(\text{ptdt})_2]$ molecules form one-dimensional columns along the *a* axis, having short intermolecular transverse S...S contacts. The crystal exhibited an extremely high electrical conductivity (7 S cm^{-1}) at room temperature as a neutral molecular crystal. High-pressure resistivity measurements was made up to 72 kbar. But contrary to usual low-dimensional organic conductors, the resistivity could not be suppressed by applying high pressure. The tight-binding band structure calculation indicated that the HOMO (highest occupied molecular orbital) and LUMO (lowest unoccupied molecular orbital) form "the crossing bands," whose Fermi surfaces tend to be vanished by HOMO-LUMO interactions. Only very small electron and hole pockets appear in the Fermi surface owing to the transverse interactions between neighboring columns. Based on these analyses, the requirements for the design of molecular metals composed of single molecules have been clarified.

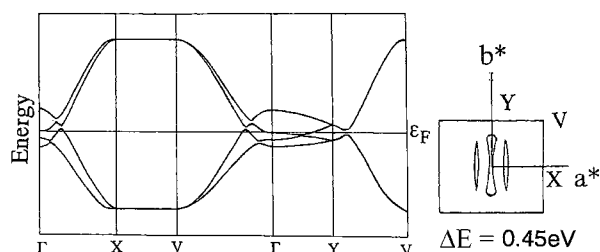


Figure 1. Tight-binding band of neutral $[\text{Ni}(\text{ptdt})_2]$ crystal. The Energy difference between HOMO and LUMO is tentatively assumed to be 0.45 eV.

IV-I-6 Structural, Electrical and Magnetic Properties of Low-dimensional Conductors Based on Unsymmetrical π Donor EDT-TTF and Analogous Selenium-substituted Molecules

SATO, Akane; KOBAYASHI, Hayao; KOBAYASHI, Akiko¹
(¹Univ. Tokyo)

[*J. Mater. Chem.* **9**, 2365 (1999)]

Organic conductors based on unsymmetrical π donor molecules EDT-TTF (ethylenedithiotetrathiafulvalene) or its selenium-substituted analogs (EDST, EDTS) and tetrahedral anions GaCl_4^- were prepared. The crystal structure determinations and the extended Hückel tight-binding band calculations indicated these systems to be quasi-one dimensional conductors similar to TMTTF or TMTSF systems (TM systems). Electrical resistivity and magnetic susceptibility measurements and low-temperature X-ray diffraction experiments suggested the spin-Peierls ground state of $(\text{EDT-TTF})_2\text{GaCl}_4$. $(\text{EDST})_2\text{GaCl}_4$ and $(\text{EDTS})_2\text{GaCl}_4$ exhibited metallic behavior down to *ca.* 40 K. The electric and magnetic properties of $(\text{EDST})_2\text{GaCl}_4$ suggested a semimetallic state at low temperature. In spite of the similarity in the crystal and electronic band structures between TM and EDT systems, these two series of quasi-one dimensional conductors do not share the same "generalized phase diagram." The electron-lattice interaction seems to be important in EDT conductors. The electric and magnetic properties of the isostructural systems with magnetic FeCl_4^- anions were also examined. The magnetic interaction between the high-spin Fe^{3+} ions was found to be very weak.

IV-J Development of Pulsed Field Gradient NMR Spectroscopy

Pulsed field gradient spin echo (PGSE) nuclear magnetic resonance (NMR) is a powerful method for the study of dynamics in condensed matter since it probes translational motion of molecules selectively, without being affected by vibrational or rotational motions. Due to this advantage it has been widely applied to the dynamics of molecules in liquids. However, applications of this technique to strongly dipole-coupled spin systems with short T_2 or to the study of slow and anisotropic self-diffusion are still challenging works because combined techniques of line-narrowing, pulsing of sharp and intense field gradients, and two-dimensional field-gradient generation are necessary.

In the present study we applied the technique to the study of anisotropic self-diffusion in liquid crystals, with the use of the laboratory-made spectrometer equipped with a rotatable quadrupole gradient coil.

IV-J-1 Self-diffusion Coefficients of a Reentrant Liquid Crystal CBOBP

OISHI, Osamu; MIYAJIMA, Seiichi

Self-diffusion coefficient tensors of a reentrant liquid crystal CBOBP were measured in the high and low temperature S_A phases. In the high temperature S_A phase, the diffusion coefficient component $D_{//}$ is larger than D_{\perp} . The two activation energies are similar. This property resembles that of the nematic phase, and indicates that the layer structure of the high temperature S_A phase is disordered remarkably. In the low temperature S_A phase, absolute values of the self-diffusion coefficient components, $D_{//}$ and D_{\perp} , are close to each other, in contrast with the diffusion coefficient components in the high temperature S_A phase. The activation energy for $D_{//}$ is much higher than that for D_{\perp} . This suggests a firm layer structure. It is also interesting to note that the activation energies for D_{\perp} are similar in the high and low temperature S_A phases, and the values of D_{\perp} are found on one straight line through both phases. Taking these in mind there seems to be no change in molecular interaction and molecular arrangement in the two S_A phases, as far as the perpendicular components concern. The change in molecular interaction and structure seemed to have occurred in the parallel components.

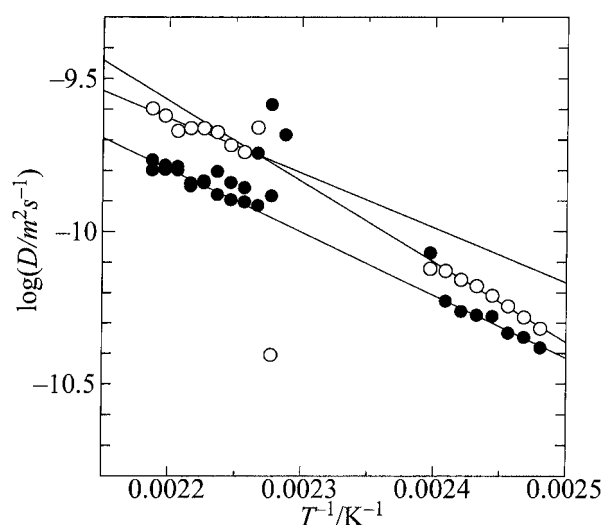


Figure 1. Anisotropic self-diffusion coefficients of CBOBP in smectic A phases (\circ $D_{//}$, \bullet D_{\perp}).

IV-J-2 Self-diffusion Coefficients of OBBC and OBBF

OISHI, Osamu; MIYAJIMA, Seiichi

OBBC is a reentrant liquid crystal. OBBF is a derivative of OBBC, where the terminal cyano group in OBBC is replaced by fluorine, and shows no reentrant phases. In the S_A phase of OBBC between the two nematic phases, the self-diffusion coefficient component $D_{//}$ is larger than D_{\perp} . The activation energies for both $D_{//}$ and D_{\perp} are low, and similar in magnitudes.

OBBF exhibits a remarkable feature. $D_{//}$ is higher than D_{\perp} , and the relative magnitudes of $D_{//}$ and D_{\perp} reverses with the change of temperature. The self-diffusion property in the S_A phase of OBBC resembles that in the high temperature phase of CBOBP, and the self-diffusion property of OBBF is close to that of the low temperature phase of CBOBP.

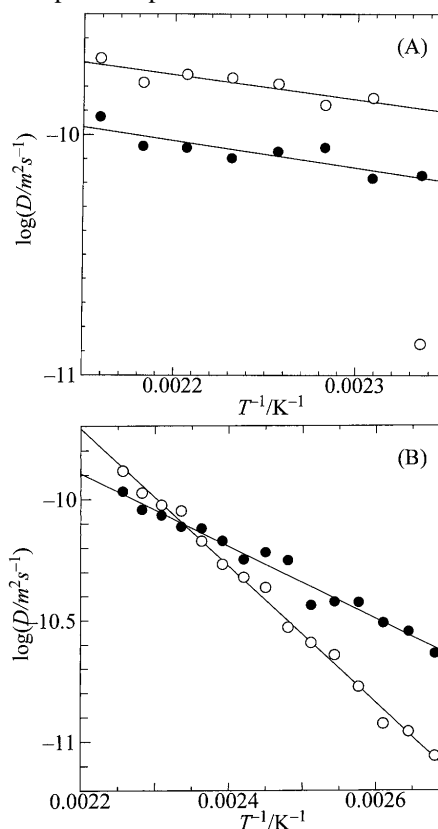


Figure 1. Anisotropic self-diffusion coefficients of OBBC(A) and OBBF(B) in smectic A phases (\circ $D_{//}$, \bullet D_{\perp}).

IV-J-3 Self-Diffusion Coefficients of an Anti-Ferroelectric Liquid Crystal MHPOBC

OISHI, Osamu; MIYAJIMA, Seiichi

The anti-ferroelectric liquid crystal MHPOBC shows various phase structures with temperature change. It was found that the activation energy for $D_{//}$ was much higher than that for D_{\perp} even in the para-electric S_A phase, and so the formation of a firm layer structure was indicated. Smaller values of $D_{//}$ indicate that diffusion across the layers is difficult.

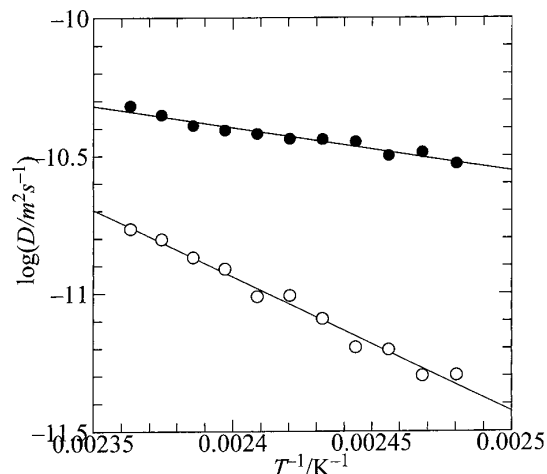


Figure 1. Anisotropic self-diffusion coefficients of MHPOBC in smectic A phase (\circ $D_{//}$, \bullet D_{\perp}).

IV-J-4 Self-diffusion Coefficients of a Hexatic Liquid Crystal PHOAB

OISHI, Osamu; MIYAJIMA, Seiichi

PHOAB exhibits a phase transition sequence, S_A — hexatic smectic B — crystalline smectic B, on lowering the temperature. In the S_A phase, the activation energy for $D_{//}$ is much higher than that for D_{\perp} . This fact shows that a firm layer structure is formed. At the phase transition from S_A to hexatic B, the self-diffusion coefficients become small to a level where even the perpendicular component was immeasurable. The diffusion properties of PHOAB and OBBF are similar: $D_{//}$ and D_{\perp} have similar values at high temperature, but

$D_{//}$ becomes smaller in comparison with D_{\perp} at low temperature.

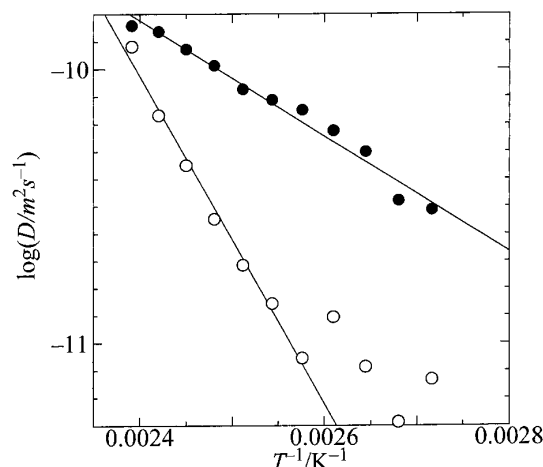


Figure 1. Anisotropic self-diffusion coefficients of PHOAB in smectic A phase (\circ $D_{//}$, \bullet D_{\perp}).

IV-J-5 Calculation of Dipole Moments by MOPAC7

OISHI, Osamu; MIYAJIMA, Seiichi

Dipole moments were calculated with the MOPAC7 program. The calculated values are 5.8 (OBBC), 4.2 (OBBF), 6.4 (CBOBP), 2.5 (MHPOBC), and 4.3 (PHOAB) Debyes. The reentrant nematic liquid crystals, OBBC and CBOBP, have larger dipole moments.

IV-J-6 Measurement of Anisotropic Self-Diffusion Coefficient Tensors by PGSE-NMR

MIYAJIMA, Seiichi; OISHI, Osamu

[*DIM Newsletter* 12, 16 (1998)]

A review account is given for the pulsed field gradient spin echo (PGSE) NMR technique, which has been applied to the determination of anisotropic self-diffusion coefficient tensors. Principles and methods are explained, and their applications to the translational dynamics of liquid crystals is presented.

IV-K Phase Transitions and Dynamical Ordering in Liquid Crystals

Extensive high resolution NMR studies were conducted to reveal the dynamics and the microscopic origin of antiferroelectricity in liquid crystals.

IV-K-1 A Bent and Asymmetrically Hindered Chiral Alkyl Chain of an Antiferroelectric Liquid Crystal as Observed by ^2H NMR

YOSHIDA, Shohei¹; JIN, Bo¹; TOKUMARU, Koh¹; TAKANISHI, Yoichi¹; ISHIKAWA, Ken¹; TAKEZOE, Hideo¹; FUKUDA, Atsuo²; KUSUMOTO, Tetsuo³;

NAKAI, Toshihito⁴; MIYAJIMA, Seiichi
(¹Tokyo Inst. Tech.; ²Shinshu Univ.; ³Sagami Cent. Res. Cent.; ⁴Tokyo Univ. Agric. Tech.)

[*J. Phys. Soc. Jpn.* 68, 46 (1999)]

The structure and dynamics of the alkyl chains are

investigated by ^2H -NMR for specifically deuterated samples of an antiferroelectric liquid crystal MHPOBC. The ^2H -NMR spectrum for the chiral alkyl chain exhibits very small quadrupolar splittings, and the methylenes close to the chiral center give double splittings, which are ascribable to two different quadrupolar splittings for each methylene unit. The unusual nature of the chiral chain is revealed; the chain is bent from the molecular long axis, and its motion is asymmetrically hindered.

IV-K-2 Experimental Spectroscopy of Liquid Crystals, No. 4-6. NMR Spectroscopy, Pt. 1-3

MIYAJIMA, Seiichi; NAKAI, Toshihito¹
(¹Tokyo Univ. Agric. Tech.)

[EKISHO 3, 43, 124 and 205 (1999)]

NMR study of liquid crystals is outlined in a series of lectures, with special emphasis on its methodological

aspects. Pt. 1 describes the theoretical framework for the spectral analysis, in connection with the orientational order parameters. Pt. 2 deals with various aspects of experimental ^{13}C NMR spectroscopy. Determination of the order parameters by the alignment-induced shifts, and determination of the nuclear shielding tensor elements by two-dimensional (2-D) site-separated spinning sideband spectroscopy are described. Use of partially averaged ^{13}C - ^1H dipolar interactions is shown in the experiments of transient oscillation in cross-polarized magnetization, and 2-D dipolar separated-local field spectroscopy. Analysis of molecular rotational motion by relaxation measurements is also shown. Pt. 3 describes how ^2H NMR is applied to solve various important problems of liquid crystals, such as determination of segmental order parameters, detection of asymmetrical hindrance in rotational motions, and detection of the phase biaxiality. Finally the pulsed field gradient spin-echo NMR technique is explained, and it is shown how the translational self-diffusion coefficient tensor elements are determined.

IV-L Electronic Properties of Alkali-Hydrogen-Carbon Systems

In alkali-hydrogen-carbon ternary systems, hydrogen or alkali metal elements exhibit a variety of electronic states when doped or intercalated in the host crystal lattice. An interesting feature is how the hydrogen 1s state contribute to the bulk electronic properties. Structural and electronic properties were studied for stage-6 sodium-hydrogen-graphite ternary compound by means of solid state NMR. New alkali-hydrogen- C_{70} compounds were synthesized by detecting and controlling the reaction of alkali hydrides with C_{70} crystal with *in-situ* ^1H NMR measurements and characterized the structures and the magnetic properties by powder X-ray diffraction, ESR and magnetic susceptibility measurements. New alkali-hydrogen-single-walled carbon nanotube aggregates were synthesized and characterized by solid state NMR.

IV-L-1 NMR Study of Stage-6 Sodium-Hydrogen-Graphite Intercalation Compound

OGATA, Hironori; MIYAJIMA, Seiichi; ENOKI, Toshiaki¹; ANTOINE, Laurence²; GUERARD, Daniel²

(¹Tokyo Inst. Tech.; ²Univ. Nancy I)

^{23}Na , ^1H and ^{13}C NMR have been carried out for stage-6 sodium-hydrogen-graphite intercalation compound (NaH-GIC). Figure 1 shows the ^1H decoupled ^{13}C NMR spectra in stage-6 NaH-GIC with the external field (B_0) perpendicular (a) and parallel (b) to the c -axis. The lines 1α and 1β correspond to the inequivalent two carbon atoms on the bounding layer (layer 1), and 2α , 2β and 3α , 3β correspond to those on middle and interior layer (layer 2 and 3), respectively. From the anisotropic values of ^{13}C NMR shifts, the charge transfer rates per one carbon atom were estimated to be 0.028, 0.005 and 0.001 for layer 1, 2 and 3, respectively. Figure 2 shows the angular dependence of the ^1H NMR second moment $\langle\Delta\nu^2\rangle$ measured at room temperature. $\langle\Delta\nu^2\rangle$ has its minimum at around 40° , which suggests that hydrogen forms two-dimensional lattice in the intercalate. However, the values of $\langle\Delta\nu^2\rangle$ obtained were much larger than those expected from the model calculation. This fact suggests

the existence of paramagnetic defects in the intercalate, which was reported for higher stage NaH-GIC sample by ESR measurement. The angular dependence of ^{23}Na NMR spectrum showed the existence of two Na^+ sites with different electric field gradient tensors.

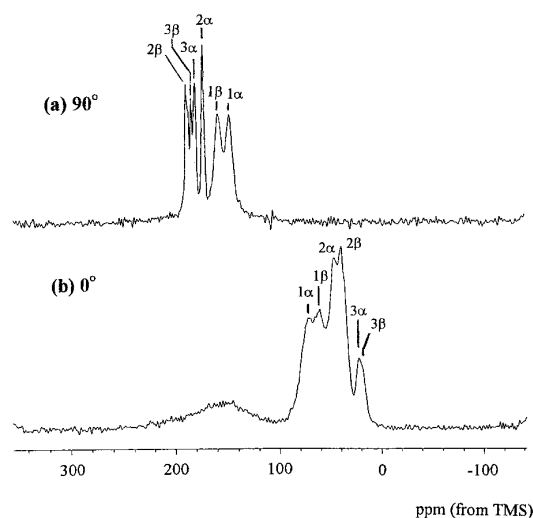


Figure 1. ^1H decoupled ^{13}C NMR spectra in stage-6 NaH-GIC with the external field (B_0) perpendicular (a) and parallel (b) to the c -axis.

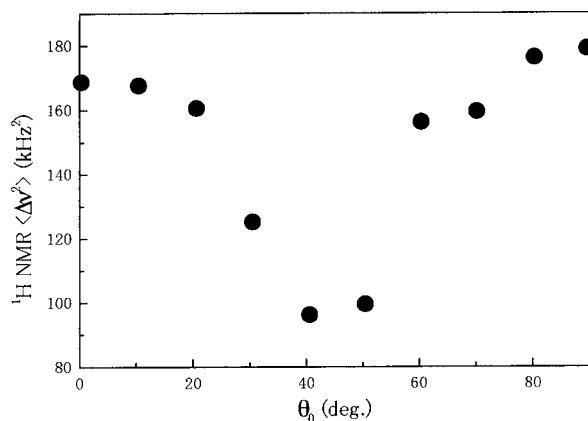


Figure 2. Angular dependence of the ${}^1\text{H}$ NMR second moment in stage-6 NaH-GIC measured at room temperature.

IV-L-2 *In-situ* NMR Study of the Reaction Process in Alkali-Hydrogen-Fullerene Systems

OGATA, Hironori

In the previous work, we have reported the attempts at detecting and controlling the reaction of potassium hydride (KH) or sodium hydride (NaH) with C_{60} crystal with *in-situ* ${}^1\text{H}$ NMR measurements. We also conducted with those of NaH or KH with C_{70} crystal. Figure 1 shows the time dependence of ${}^1\text{H}$ NMR spectra for a mixture of stoichiometric amounts (3:1) of NaH and C_{70} reacted at 503 K (a) and of KH and C_{70} at 450 K (b), respectively. After several minutes' reaction, a signal at about -4 ppm appeared, which may be ascribable to decomposition of KH or NaH. Just after the intensity of this peak became maximum, the sample was cooled rapidly to 150 K to stop the reaction. After cooling, the hydrogen peak disappeared for NaH- C_{70} sample but stabilized as hydrogen anion for KH- C_{70} sample. This peak intensity, however, gradually decreased after the sample was heated up to room temperature and disappeared within 24 hrs. Powder X-ray diffraction profile of the KH- C_{70} sample just after the reaction showed that these crystals form fcc structure with lattice constant $a = 15.04 \text{ \AA}$ at room temperature. This value is larger than that of fcc K_3C_{70} ($a = 14.96 \text{ \AA}$ at room temperature). These facts suggest that hydrogen anion is occupied in the interstitial site of the K_3C_{70} crystal just after the reaction. Figure 2 shows the temperature dependence of the magnetic susceptibility of $\text{K}_3\text{H}_x\text{C}_{70}$ just after the reaction. A small but distinct anomaly, which was not reported for K_3C_{70} was observed at 120 K. This anomaly was also observed in the temperature dependence of ESR peak-to-peak linewidth ($\Delta H_{\text{p-p}}$) for $\text{K}_3\text{H}_x\text{C}_{70}$ (Figure 3). The value of Pauli-paramagnetic susceptibility was evaluated to be about 7×10^{-4} emu/mole from ESR and magnetic susceptibility measurements.

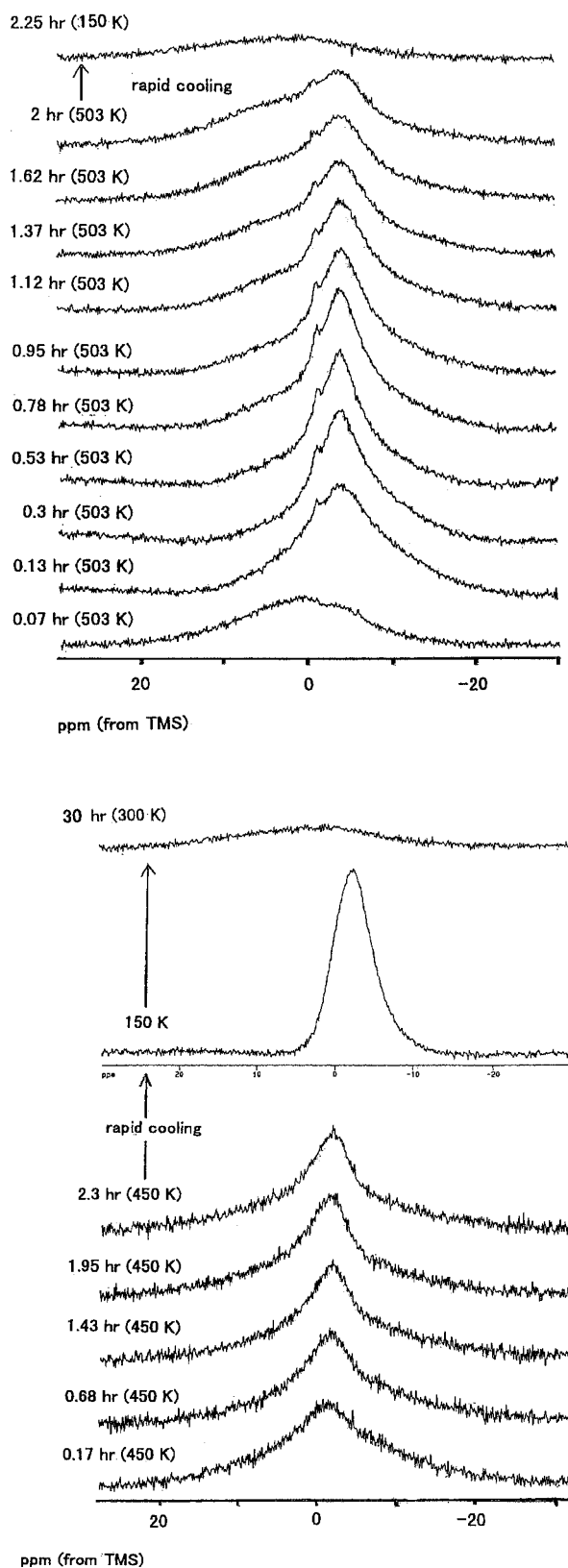


Figure 1. Time dependence of *in-situ* ${}^1\text{H}$ NMR spectra for the mixture of (a) NaH and C_{70} and of (b) KH and C_{70} .

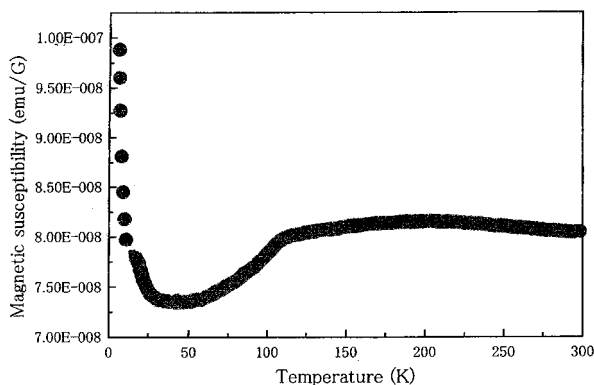


Figure 2. Temperature dependence of static magnetic susceptibility of $K_3H_xC_{70}$ just after the reaction.

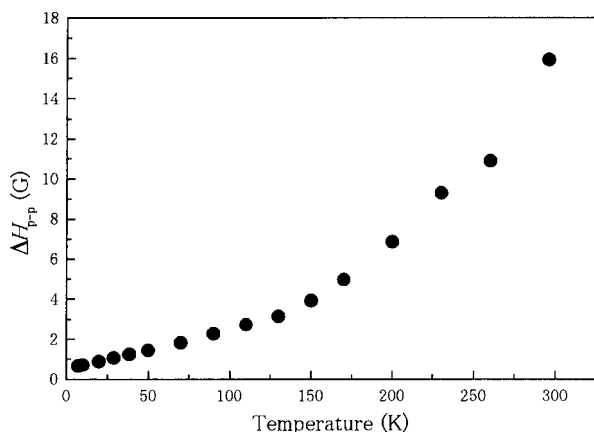


Figure 3. Temperature dependence of ESR peak-to-peak linewidth for $K_3H_xC_{70}$ just after the reaction.

IV-L-3 Synthesis and NMR study of Alkali-Hydrogen-Single-Walled Carbon Nanotubes

OGATA, Hironori; BANDOW, Syunji¹; KUNO, Syougo²; SAITO, Yahachi²
(¹ICORP-JST; ²Mie Univ.)

Potassium-hydrogen-single-walled carbon nanotubes (K-H-SWNTs) aggregates were synthesized first and their states of hydrogen were studied by solid state ¹H NMR. Rh-Pt mixed catalysts and hydrogen peroxide were used to produce SWNTs and remove amorphous carbon particles in the raw soot. Two kinds of SWNTs were prepared as starting sample, one was the SWNTs with caps and the other was those without caps obtained by a heating treatment in dried air. K-H-SWNTs samples were synthesized by both (a) the direct reaction of potassium hydride (KH) and SWNTs and (b) the absorption of H₂ gas on K-doped SWNTs. ¹H NMR measurements proved that a singlet ¹H spectrum with the value of the second moment of about 40 kHz² at -10 ppm (from TMS) was observed only by using uncapped SWNTs as starting samples, independently of the way of synthesis. This fact suggests that hydrogen anion is condensed inside SWNTs for K-H-SWNTs (uncapped) system.

IV-M Structural and Electronic Properties of New Carbon Materials

Electronic properties and the function of micropores were studied for new carbon materials in this project. ¹³C NMR were performed first for single-walled carbon nanotubes (SWNTs) to investigate the electronic structure in the magnetic field. The behavior of water molecules absorbed in activated carbon fiber (ACF) was studied by solid state ¹H NMR.

IV-M-1 ¹³C NMR Study of Single-Walled Carbon Nanotubes

OGATA, Hironori; BANDOW, Syunji¹; KUNO, Syougo²; SAITO, Yahachi²
(¹ICORP-JST; ²Mie Univ.)

¹³C NMR experiments have been carried out for single-walled carbon nanotubes (SWNTs), which were produced by using non-ferromagnetic Rh-Pt mixed catalysts. Hydrogen peroxide was used to remove amorphous carbon particles in the raw soot almost perfectly. Figure 1 shows the ¹³C NMR spectrum at 298 K. From the line shape analysis of the ¹³C spectrum, the shift tensor was evaluated to be (δ_{11} , δ_{22} , δ_{33}) = (192, 186, 132) ppm. Small anisotropic value ($\Delta\delta = -57$ ppm) compared with that reported for MWNTs¹) suggests that this SWNTs sample contains metallic tubes with larger electronic density of states at the Fermi level than that

of MWNTs sample. Furthermore, the intensity of ¹³C signal was found to be weak for the amount of the sample, suggesting that the ¹³C signal observed was only from metallic tubes. The ¹³C NMR signal of semi-conducting tubes was broadened and could not be observed virtually due to the large anisotropy of diamagnetic susceptibility, which is theoretically predicted.²⁾

To obtain more detailed information about the electronic state of SWNTs, we performed ¹³C spin lattice relaxation time (T_1) measurement at 100.1 MHz (9.4 T). Figure 2 shows the temperature dependence of spin-lattice relaxation time at 9.4 T. It is found that SWNTs follows a Korringa-like behavior ($T_1 \times T = 940 \pm 60$ (sec.K)) in the temperature region between 4.2 K and 100 K, which is different largely with that of graphite sample.³⁾ This fact suggests that metallic tubes exist at the magnetic field of 9.4 T.

References

- 1) Y. Maniwa *et al.*, *Proc. XII Int. Winterschool* (Kirchberg, Austria) 87 (1998).
- 2) Ajiki and Ando, *J. Phys. Soc. Jpn.* **62**, 2470 (1993).
- 3) K. Kume *et al.*, *Synth. Met.* **12**, 307 (1985).

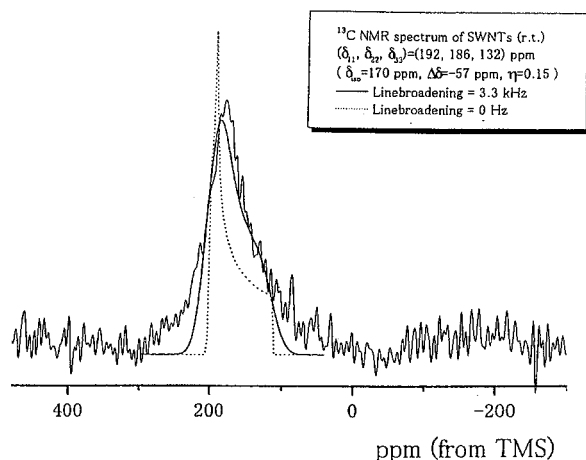


Figure 1. ^{13}C NMR spectrum of SWNTs at 298 K.

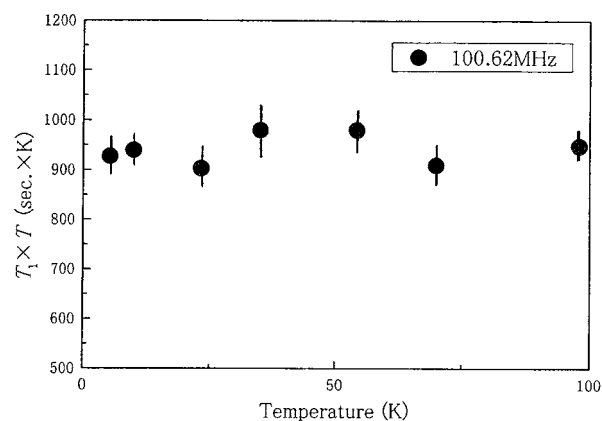


Figure 2. Temperature dependence of ^{13}C $T_1 \times T$ of SWNTs at 9.4 T.

IV-M-2 Dynamics of Water Molecules Confined in Activated Carbon Fiber

OGATA, Hironori; MIYAJIMA, Seichi; YOSHIKAWA, Yuuhi¹; SATO, Hirohiko¹; ENOKI, Toshiaki¹
(¹Tokyo Inst. Tech.)

Water molecules adsorbed in microporous carbon materials are expected to show distinctive characteristics different from those in the bulk state. For example, since micrographite surfaces in carbon materials are hydrophobic, if water is adsorbed, its structure is essentially affected by either the confinement effect or the hydrophobic effect originating in the interaction with carbon surfaces. ^1H NMR measurements were conducted for water molecules adsorbed in activated carbon fiber (ACF). At room temperature the lineshape of the ^1H NMR spectrum for this system consists of two peaks at -0.4 ppm and -3.9 ppm (from TMS) with

inhomogeneous broadenings, which are considered to be attribute to the difference of the adsorption sites of water molecules. The temperature dependence of the value of the ^1H NMR second moment ($\langle \Delta v^2 \rangle$) is shown in Figure 1. With decreasing temperature, $\langle \Delta v^2 \rangle$ increased drastically at about 190 K and a plateau of 55 kHz^2 was observed below 160 K, which was much smaller than that of bulk ice (about 345 kHz^2 at 200 K). The peak position of the ^1H NMR spectrum at 160 K was +10 ppm. These facts suggests that water molecules confined in ACF micropores freeze and form a hydrogen-bonded network at 160 K and that strong interaction between water molecules and ACF micropores surface hinders the the growth of three-dimensional hydrogen-bonded network. Figure 2 shows the temperature dependence of ^1H NMR spin-lattice relaxation time (T_1) for this system. The distinct minimum of the T_1 at 225 K was observed, which is thought to be associated with the self-diffusion of the water molecules. The activation energy (E_a) and the correlation time (τ_c) at 298 K were evaluated to be 2.7 kcal/mole, and 5.5×10^{-11} sec., respectively. The value of E_a obtained is almost same as that of the self-diffusion for bulk water (4 kcal/mole), however, the value of τ_c is much larger than that of bulk water (2.5×10^{-12} sec. at 298 K) due to the confinement effect.

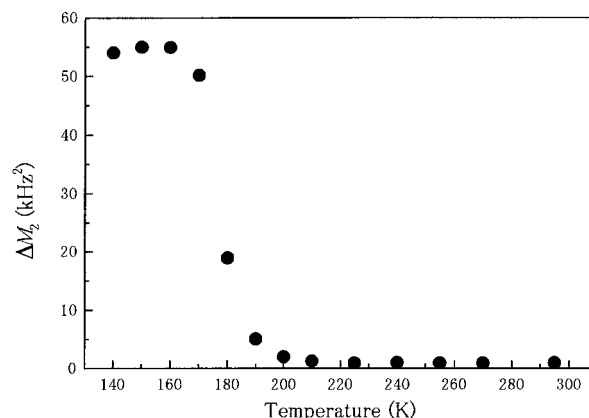


Figure 1. Temperature dependence of ^1H NMR second moment for water adsorbed activated carbon fiber.

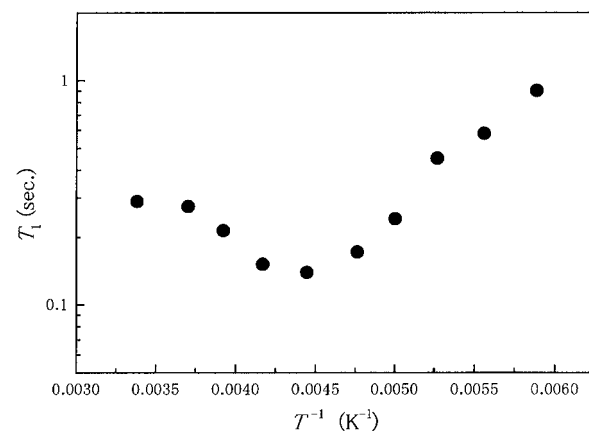


Figure 2. Temperature dependence of ^1H NMR spin-lattice relaxation time for water adsorbed activated carbon fiber.

IV-N Structural and Electronic Properties of Fullerene-Based Compounds

Structural and electronic properties were studied for several types of fullerene-based compounds in this project. Electronic and magnetic properties of $\text{Na}_x(\text{THF})_y\text{C}_{60}$ single crystals were studied by magnetic susceptibility, ESR and Raman scattering measurements. ^1H , ^{23}Na and ^{13}C NMR studies were conducted for $\text{Na}_x(\text{THF})_y\text{C}_{60}$ single crystals to reveal the microscopic origins of the phase transitions and the structural and electronic states at low temperature. Attempts at doping Ce into C_{60} crystal were conducted and structural and magnetic properties of the products were investigated. Raman scatterings and X-ray powder diffractions for a pressure induced superconductor Cs_3C_{60} were studied under some pressures.

IV-N-1 Electronic Properties of Alkali-THF- C_{60} Single Crystals

OGATA, Hironori; KOBAYASHI, Hayao; YAKUSHI, Kyuya; MORIYAMA, Hiroshi¹
(¹Toho Univ.)

The electronic and magnetic properties of $\text{Na}_x(\text{THF})_y\text{C}_{60}$ single crystals were studied by means of ESR, magnetic susceptibility, and Raman scattering measurements. Figure 1 shows the temperature dependence of ESR peak-to-peak linewidth ($\Delta H_{\text{p-p}}$) for $\text{Na}_x(\text{THF})_y\text{C}_{60}$. The value of $\Delta H_{\text{p-p}}$ decreases monotonically with decreasing temperature in the temperature region between 300 K and 10 K with sudden drop at 180 K. This drop is attributed to be metal-metal phase transition previously reported for this compound.¹⁾ Pauli susceptibility at room temperature was evaluated to be $\chi_{\text{P}} = 3.6 \times 10^{-4}$ (emu/mol) from ESR measurement. Figure 2 shows the temperature dependence of magnetic susceptibility for $\text{Na}_x(\text{THF})_y\text{C}_{60}$. Two small reduction in the magnetic susceptibility were observed below 180 K and 50 K, the former is attributed to be metal-metal phase transition above-mentioned. The temperature dependence of the peak position of the $A_{\text{g}}(2)$ mode of C_{60} in $\text{Na}_x(\text{THF})_y\text{C}_{60}$ revealed that the molecular valence of C_{60} was -1 in the temperature region between 298 K and 4.2 K. In conclusion, it was found that $\text{Na}_x(\text{THF})_y\text{C}_{60}$ is a metal down to 4.2 K, which is composed of C_{60}^{1-} anions.

Reference

1) H. Kobayashi *et al.*, *J. Am. Chem. Soc.* **116**, 3153 (1994).

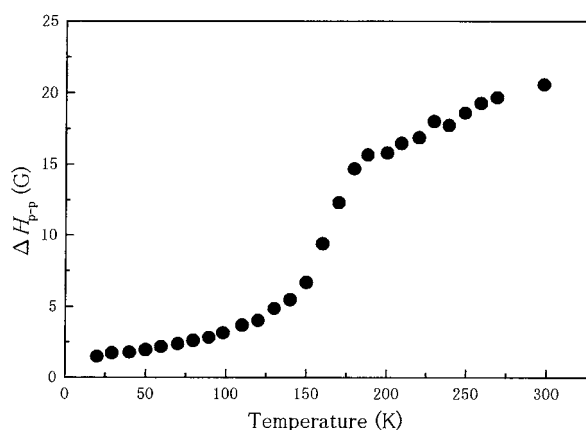


Figure 1. Temperature dependence of ESR peak-to-peak linewidth ($\Delta H_{\text{p-p}}$) for $\text{Na}_x(\text{THF})_y\text{C}_{60}$ single crystals.

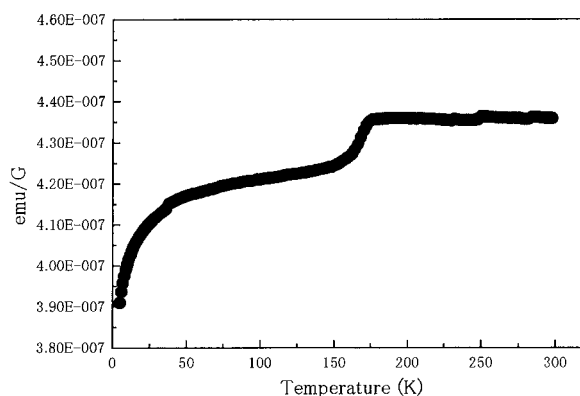


Figure 2. Temperature dependence of magnetic susceptibility for $\text{Na}_x(\text{THF})_y\text{C}_{60}$ single crystals.

IV-N-2 NMR Study of Sodium-THF- C_{60} Single Crystals

OGATA, Hironori; KOBAYASHI, Hayao; MORIYAMA, Hiroshi¹
(¹Toho Univ.)

^1H , ^{23}Na and ^{13}C NMR measurements were performed for $\text{Na}(\text{THF})_y\text{C}_{60}$ single crystals to elucidate the microscopic origins of the phase transitions at 180 K and 50 K and the electronic state at low temperature. Figure 1 shows the temperature dependence of ^{23}Na NMR spectrum for $\text{Na}(\text{THF})_y\text{C}_{60}$. A singlet spectrum appearing at -7 ppm (from 1.0 M NaCl aq. sol.) at 297 K suggests that more than four THF molecules are coordinated around the Na^+ ions. The ^{23}Na linewidth does not undergo the remarkable change at 180 K, while the line broadening is observed below 50 K. Figure 2 shows the temperature dependence of ^1H NMR spectrum for $\text{Na}(\text{THF})_y\text{C}_{60}$. The ^1H linewidth changed clearly at 180 K. At 160 K, the linewidth of ^1H NMR spectrum ($\Delta H_{1/2}$) is evaluated to be about 8 G, which is smaller than that of motionless THF molecules (~ 15 G). No significant change was observed at 180 K in the temperature dependence of the line shape of ^{13}C NMR spectrum. These facts are explicable by assuming that the librational motion around the axis connecting between sodium cation and the oxygen of the THF molecule freezes below 180 K and the hydrogen of the $-\text{CH}_2-$ group becomes motionless below 50 K in the time scale of NMR. The temperature dependence of the ^{13}C nuclear spin-lattice relaxation rate, T_1^{-1} , exhibited Korringa-like behavior ($T_1 \times T = 550$ (sec \times K)) in the temperature region between 50 K and 6 K. This facts suggests that $\text{Na}(\text{THF})\text{C}_{60}$ is metallic down to 6 K. The

electronic density of states at Fermi level of this compound was evaluated to be about 30% of that of K_3C_{60} superconductor, provided that these electronic correlation effects are equal.

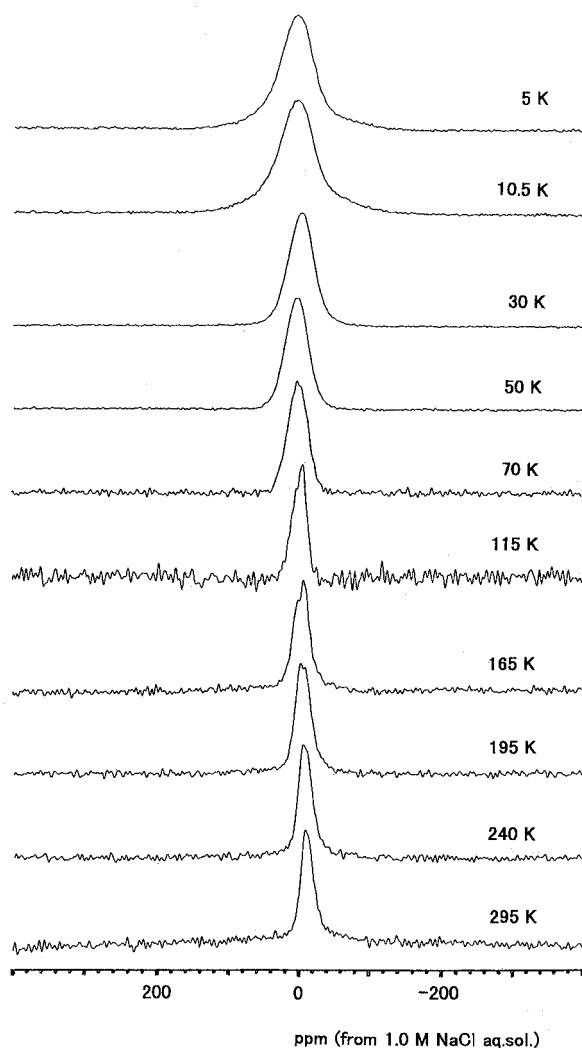


Figure 1. Temperature dependence of of ^{23}Na NMR spectrum for $\text{Na}(\text{THF})_y\text{C}_{60}$ single crystals.

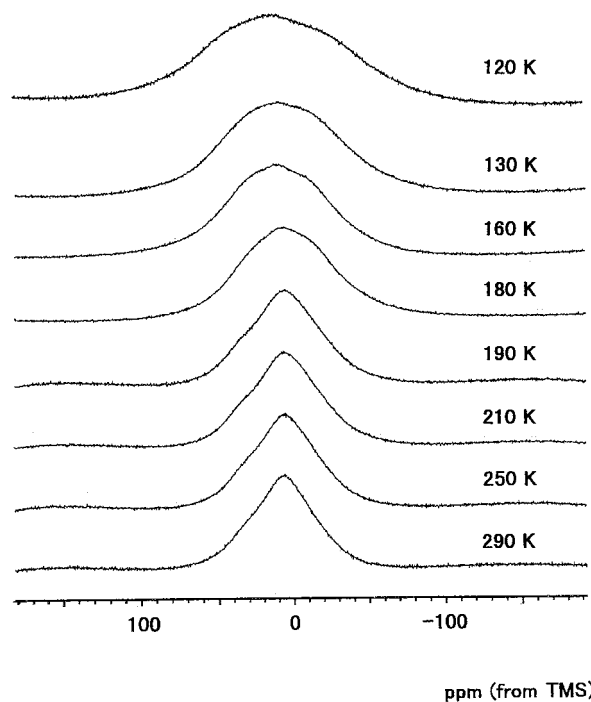


Figure 2. Temperature dependence of of ^1H NMR spectrum for $\text{Na}(\text{THF})_y\text{C}_{60}$ single crystals.

IV-N-3 Magnetic Behaviors of High-Temperature Reaction Products of Cerium Metal and C_{60} Solid

MARUYAMA, Yusei¹; SUZUKI, Kenji¹; TAKAGI, Sigenori¹; MOTOHASHI, Satoru¹; OGATA, Hironori
(¹Housei Univ.)

Exohedral metal doping or intercalation to C_{60} solids has been known to be a very important method to modify the solid state properties of C_{60} dramatically. In this study we have used Ce metal as the dopant which has the lowest melting point, 1072 K, among the lanthanide elements and has relatively low ionization potential, 5.54 eV, because it might react with C_{60} solid in the liquid state. Ce metal powder and C_{60} powder were mixed at the nominal stoichiometry of (1.5-1.8):1 in a quartz tube under argon atmosphere and sealed off with 50 Torr He gas after evacuation. The samples were heated in an electric furnace at 650, 700, 750, 800, 850, 900 and 1100 °C for several to 10 hours respectively. The temperature dependence of the magnetizations clearly shows the existence of ferromagnetism in these samples which could be originated in the $4f^1$ electrons of Ce^{3+} ions. Figure 1 shows the M - T curve for 650 °C sample. The ZFC curve in Figure 1 is indicating the diamagnetic contribution in the temperature region of 5–15 K against the ferromagnetic uptake of the magnetization. The M - T curve for 1100 °C sample is shown in Figure 2. Negative magnetization is clearly observed below 10.5 K in the ZFC curve as shown in Figure 2, which may indicate the occurrence of superconductivity in this system.

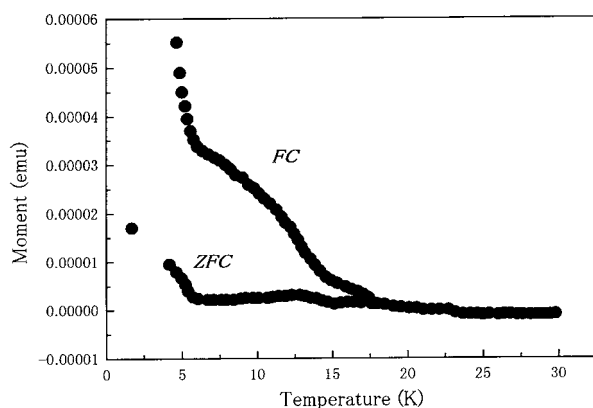


Figure 1. M - T curve of $Ce_{1.5}C_{60}$ reacted at 650 °C.

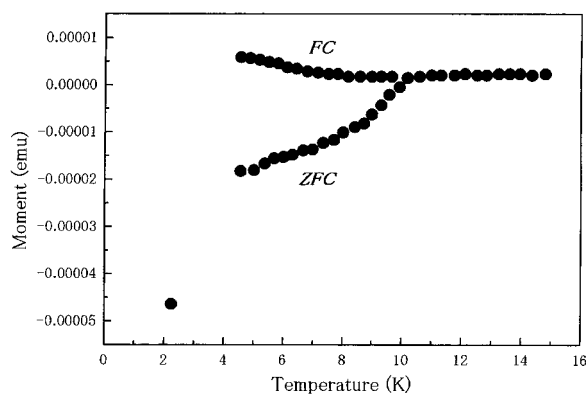


Figure 2. M - T curve $Ce_{1.5}C_{60}$ reacted at 1100 °C.

IV-N-4 Structure and Raman Scatterings of Cs_3C_{60} under High Pressure

FUJIKI, Satoshi¹; KUBOZONO, Yoshihiro¹;
 TAKABAYASHI, Yasuhiro¹; KASHINO, Setsuo¹;
 EMURA, Shuichi²; FUJIWARA, Akihiko³; ISHII,
 Kenji³; SUEMATSU, Hiroyoshi³; MURAKAMI,
 Youichi⁴; IWASA, Yoshihiro⁵; MITANI, Tadaaki⁵;
 OGATA, Hironori
 (¹Okayama Univ.; ²Osaka Univ.; ³Univ. Tokyo; ⁴KEK-
 PF; ⁵JAIST)

Raman scatterings for a pressure induced superconductor Cs_3C_{60} were studied in a pressure region from 1 bar to 62 kbar. The center frequency ω_0 for $H_g(1)$ and $H_g(2)$ Raman peaks increased by applying pressure, but it showed a saturation in high pressure region. On the other hand, the ω_0 for $A_g(1)$ and $A_g(2)$ modes increased straightforwardly in all pressure region. The electron-phonon coupling constant for Cs_3C_{60} showed no increase at high pressures. X-ray powder diffraction patterns at 11 K under a pressure of 40 kbar showed that a superconducting phase for Cs_3C_{60} was body-centered orthorhombic.

IV-O Magnetic Local Structure and Magnetic Interactions in Molecule Based and Organic-Inorganic Hybrid Magnets

Organic ferromagnet is one of the realizations of great possibilities of organic molecules which can be designed to exhibit a variety of functions by chemical modifications and attracts interest of chemists in broad areas such as organic, physical, and theoretical chemistry, *etc.* Ferromagnetism of organic materials is of current interest. It is desired to clarify the mechanism of intermolecular magnetic interaction in a microscopic viewpoint to establish a leading principle to produce the ferromagnetic ordering in the crystalline phase of molecule based materials and to understanding the characters and the functions of open-cell molecules. Solid state high resolution NMR techniques provide an unique information of the magnetic local structure and the magnetic interactions in a microscopic view point. We have investigated the magnetic local structure and magnetic interaction for a variety of magnetic materials including a class of organic-inorganic hybrid magnetic materials. Botallackite-type compounds $\text{Cu}_2(\text{OH})_3\text{X}$ (X = exchangeable anion) exhibit layered structures, in which a nonequilateral planar triangular lattice of copper ions is constructed. The copper ions are bridged by hydroxide ions and exchangeable anions X to form infinite layers. A variety of anions X can be incorporated by anion-exchange in suspended solution and the bulk magnetism of $\text{Cu}_2(\text{OH})_3\text{X}$ is controlled by the property of X .

IV-O-1 Solid State High Resolution Deuterium NMR Study of Electron Spin Density Distribution of Hydrogen-bonded Organic Ferromagnetic Compound 4-Hydroxyimino-TEMPO

MARUTA, Goro¹; TAKEDA, Sadamu^{2,3}; IMACHI, Ron⁴; ISHIDA, Takayuki⁴; NOGAMI, Takashi⁴; YAMAGUCHI, Kizashi¹

(¹Osaka Univ.; ²Gunma Univ.; ³IMS; ⁴Univ. Electro-Commun.)

[*J. Am. Chem. Soc.* **121**, 424 (1999).]

Electron spin density distribution at hydrogen atoms of 4-hydroxyimino-2,2,6,6-tetramethylpiperidin-1-ylloxyl (4-hydroxyimino-TEMPO), which has been recently found to be a molecular ferromagnet at low temperature, was determined in the crystalline phase from the temperature dependence of the Fermi contact shifts of magic angle spinning deuterium NMR spectrum to elucidate the mechanism of intermolecular magnetic interaction. There are two kinds of close contacts among neighboring radical molecules in the crystalline phase. An axial methyl hydrogen atom locates closely to a neighboring N-O radical group and the hydroxyl group forms hydrogen-bonding with another neighboring N-O radical group. The plus and minus signs of observed hyperfine coupling constants A_D of methyl deuteriums indicate that two different mechanisms of electron spin density distribution exist. Equatorial CD_3 groups show negative coupling constants ($A_D = -0.24$ MHz) induced by the intramolecular spin polarization mechanism, whereas positive hyperfine coupling constants ($A_D = +0.12$ MHz) of axial CD_3 groups indicate that a single occupied MO spreads out partly toward the axial CD_3 groups by the mechanism of hyperconjugation. The small positive hyperfine coupling constant of the axial methyl group is brought about from averaging among one positive and two negative values of the three deuterium atoms of the methyl group due to rapid rotation. The intermolecular magnetic interaction through the axial methyl group seems to be sensitive to the orientation of the methyl group and it can be ferromagnetic in the crystal of 4-hydroxyimino-TEMPO. A large negative hyperfine

coupling constant ($A_D = -0.45$ MHz) observed for the NOD group strongly implies that the hydrogen-bonding mediates the intermolecular magnetic interaction in the crystalline phase. The experimental results and the molecular orbital calculations indicate that the ferromagnetic interaction exists in the hydrogen-bonded chains running along the crystallographic c axis and that the two chains are considered to be coupled ferromagnetically through the axial methyl groups to form a double chain. In the directions of crystallographic a and b axes, weak ferromagnetic interactions are expected from the measured spin density distributions of the deuterium atoms of the equatorial methyl and of the methylene groups which participate in inter-chain contacts in a crystallographic a - b plane.

IV-O-2 Magic Angle Spinning ¹H-NMR Study of the Spin Density Distribution of Pyridyl Nitronyl Nitroxides in the Crystalline Phase

MARUTA, Goro¹; TAKEDA, Sadamu^{2,3}; YAMAGUCHI, Akira⁴; OKUNO, Tsunehisa⁴; AWAGA, Kunio⁴; YAMAGUCHI, Kizashi¹

(¹Osaka Univ.; ²Gunma Univ.; ³IMS; ⁴Univ. Tokyo)

[*Mol. Cryst. Liq. Cryst.* **334**, 295 (1999)]

Electron spin density distribution was investigated for p - and m -pyridyl nitronyl nitroxides (p -PYNN and m -PYNN) in the crystalline phase by the temperature dependence of the solid state high-resolution ¹H-MAS NMR spectrum. The results were compared with that of phenyl nitronyl nitroxide (PNN) for elucidating the effect of incorporation of a nitrogen atom into the aromatic group. For p -PYNN, the magnitude of the negative spin density at 3 and 5 positions of the pyridyl group was suppressed by 30% in comparison with that of PNN and the positive spin density at 2 and 6 positions was slightly enhanced by 10%. On the other hand, the positive spin density at 2, 4 and 6 positions of pyridyl group of m -PYNN was suppressed by 30% in average and the negative one at 5 was also suppressed by 20%. The DFT calculation at UBLYP/6-31G(d,p) level suggested that the molecular geometry largely contributed to the change of the spin density in addition

to the effect of incorporation of the nitrogen atom. In fact, the spin density distribution of the aromatic ring of *p*-PYNN was remarkably reduced in solution compared with that in the crystalline phase.

IV-O-3 Local Magnetic Structure of Layered Compounds $\text{Cu}_2(\text{OD})_3\text{X}$ with Exchangeable Acid Anion X Studied by Solid State High Resolution Deuterium NMR

TAKEDA, Sadamu^{1,2}; MARUTA, Goro²; TERASAWA, Katsumasa; FUKUDA, Nobuya; YAMAGUCHI, Kizashi³

(¹Gunma Univ.; ²IMS; ³Osaka Univ.)

[*Mol. Cryst. Liq. Cryst.* **335**, 723 (1999)]

The microscopic magnetic local structure of Botallackite-type layer structured compounds $\text{Cu}_2(\text{OD})_3\text{X}$ ($\text{X} = \text{NO}_3^-$ and HCOO^-) exhibiting non-equilateral planar-triangular magnetic lattice was determined by the solid-state high-resolution deuterium NMR of deuterated hydroxy groups in the high temperature region above 190 K. The magnetic interactions in a copper ion layer were probed by the paramagnetic NMR shifts of the two chemically distinct hydroxy groups. Isotropic NMR shift of each hydroxy group showed different temperature dependence, suggesting non-uniform magnetic interaction. It appeared that the magnetic interaction in the copper layer could be decomposed to a sum of 1D-Heisenberg ferro- and antiferromagnetic chains in the high temperature region. Two distinct copper chains with ferro- and antiferromagnetic exchange interactions $J = +19 \pm 11$ and -21 ± 3 K were found for $\text{X} = \text{NO}_3^-$ from the temperature dependence of the two distinct NMR signals, while $J = +13 \pm 7$ and -13 ± 5 K for $\text{X} = \text{HCOO}^-$. The derived values of J almost reproduced the temperature behavior of the magnetic susceptibility χ_{AT} vs. T .

IV-O-4 Solid State High Resolution NMR Studies of Electron Spin Densities in Charge-Transfer Complex-Based Organic Ferromagnets

MARUTA, Goro¹; TAKEDA, Sadamu^{2,3}; YAMAGUCHI, Kizashi¹; UEDA, Kazumasa⁴; SUGIMOTO, Toyonari⁴

(¹Osaka Univ.; ²Gunma Univ.; ³IMS; ⁴Osaka Pref. Univ.)

[*Synth. Met.* **103**, 2333 (1999)]

A variety of purely organic ferromagnets, which consist of stable neutral radical species, have been developed. Charge-transfer complex-based organic ferromagnets are particularly of current interest because

of their potential to exhibit ferromagnetism at high temperatures. In these compounds, donor (D^{\bullet}) and acceptor (A^{\bullet}) can be designed to bear electron spins and electronic conduction can be also expected, so that the magnetic interaction in these salts may be different from those in neutral radical-based magnetic crystals and a novel magnetism is expected. A series of 4,4,5,5-tetramethylimidazolin-1-oxyls with 4-(*N*-R-pyridinium) groups at the 2-position (1^{\bullet} : R = methyl, 2^{\bullet} : R = ethyl, 3^{\bullet} : R = *n*-propyl) form stable charge transfer complexes with the radical anion of TCNQF₄. It has been revealed by the magnetic susceptibility measurements that $1^{\bullet}\cdot\text{TCNQF}_4^{\bullet-}$ and $3^{\bullet}\cdot\text{TCNQF}_4^{\bullet-}$ are ferromagnets at low temperature ($T_c \sim 0.5$ K), whereas $2^{\bullet}\cdot\text{TCNQF}_4^{\bullet-}$ exhibits antiferromagnetic behavior. It is interesting to study the mechanism of magnetic interaction of these CT complexes. The mechanism can be elucidated from the electron spin density distribution in the magnetic crystals. In this work, we have determined the electron spin density distribution and the magnetic local structure in the salts of $1^{\bullet}\cdot\text{TCNQF}_4^{\bullet-}$, $2^{\bullet}\cdot\text{TCNQF}_4^{\bullet-}$ and $3^{\bullet}\cdot\text{TCNQF}_4^{\bullet-}$ by solid state high resolution ¹H, ¹³C and ¹⁹F-NMR.

IV-O-5 Variable Magnetism of Layer-Structured Compounds $\text{Cu}_2(\text{OD})_3\text{X}$ with Exchangeable Anion X: Magnetic Local Structure and Magnetic Interactions Determined by Solid-State High-Resolution Deuterium NMR

TAKEDA, Sadamu^{1,2}; ARAI, Masahiro¹; MARUTA, Goro³; YAMAGUCHI, Kizashi³

(¹Gunma Univ.; ²IMS; ³Osaka Univ.)

[*Mol. Cryst. Liq. Cryst.* in press]

The microscopic magnetic local structure of Botallackite-type layer-structured compounds $\text{Cu}_2(\text{OD})_3\text{X}$ ($\text{X} = \text{C}_6\text{H}_5\text{COO}^-$) was determined by the solid-state high-resolution deuterium NMR above 190 K. The magnetic interaction in a copper layer was probed by the isotropic NMR shifts of OD⁻ groups and could be approximated by a sum of 1D-Heisenberg chains in the high temperature region. Two copper chains with different exchange interactions $J = -54 \pm 4$ and -92 ± 3 K were found for $\text{Cu}_2(\text{OD})_3\text{C}_6\text{H}_5\text{COO}$ from the temperature dependence of the three distinct NMR signals. The derived values of J almost reproduced the high temperature behavior of the magnetic susceptibility χ_{AT} vs. T . The magnetic susceptibility of isotopic analogue $\text{Cu}_2(\text{OH})_3\text{C}_6\text{D}_5\text{COO}$ showed ferromagnetic interaction below 50 K. Electron spin distribution in a phenyl ring of a benzoate anion is governed by spin polarization mechanism and its magnitude is very small. Magnetic interaction between the layers through the benzoate anion is very weak.

IV-P Proton Transfer Tunneling in Interacting Hydrogen Bonds in the Solid State

Control of functional interactions, such as electronic and dynamic one, is a key to produce new functional materials. It is important to study the possibility of the functional interactions in the solid state. The nuclear magnetic resonance provides microscopic aspects of the functional interactions in the solid state. Hydrogen bond has a great capability for mediating a variety of interactions. We have investigated proton transfer dynamics in the interacting hydrogen bonds in organic quasi-conjugated π -system. Interaction between the hydrogen bonds is a key point for propagating an information of one hydrogen bond to the other hydrogen bond through molecular frame.

IV-P-1 Proton Dynamics in Interacting Hydrogen Bonds in the Solid State: Proton Tunneling in the NHO Hydrogen Bonds of N,N'-Di(2-Hydroxy-1-Naphthylmethylene)-*p*-Phenylenediamine

TAKEDA, Sadamu^{1,2}; INABE, Tamotsu³; BENEDICT, Claudia⁴; LANGER, Uwe⁴; LIMBACH, Hans-Heinrich⁴
(¹Gunma Univ.; ²IMS; ³Hokkaido Univ.; ⁴Freie Univ., Berlin)

[*Ber. Bunsen-Ges.* **102**, 1358 (1998)]

Combination of comprehensive investigations of the spin-lattice relaxation rate of proton and low temperature ¹⁵N-CP/MAS NMR spectrum provides unique information of proton dynamics in two interacting NHO hydrogen bonds of solid N,N'-di(2-hydroxy-1-naphthylmethylene)-*p*-phenylenediamine (DNP). It was evidenced from the ¹H-NMR relaxation measurement that tunneling mechanism operates for the proton transfer in the hydrogen bonds. The tunneling phenomenon is closely related to the very small energy differences among the four tautomeric states accompanied with the proton transfer in the two NHO hydrogen bonds. The very small values of the energy difference, in spite of the chemically asymmetric NHO hydrogen bond, were revealed by the ¹⁵N-CP/MAS NMR spectrum. This is a unique character of solid DNP. It was also suggested from the derived energy scheme of the four tautomers and activation energies of the proton transfer that an interaction exists between the two NHO hydrogen bonds linked by π -electronic molecular frame. This means that the information of one NHO hydrogen bond, *e.g.* OH-form or NH-form, propagates to the other hydrogen bond and the proton transfer in one hydrogen bond induces the change of the potential function for the proton transfer in the other hydrogen bond.

IV-Q Systematic Study of Organic Conductors

Thanks to the systematic view to structure-property relationship studied particularly in BEDT-TTF-based conductors, recently our understanding of organic conductors has made a great progress. From the concept of “universal phase diagram” in the θ -phase, we can predict metal-insulator transition temperatures of a large number of organic conductors. The underlying logic behind this universal view has been explained by the change of orbital overlap between adjacent molecules. Systematization of detailed stacking patterns in the β - and β' - phases has attempted, from which we can make a fairly good prediction to superconducting phases. These universal views are applied to individual cases, in particular to β -(BEDT-TTF)₂PF₆ family salts with twisted overlap mode, and to α' -phase salts, which are regarded as hybrid of the θ - and β' -phases, and actually whose properties are a complicated mixture of these parent phases.

IV-Q-1 Structural Genealogy of BEDT-TTF-Based Organic Conductors I. Parallel Molecules: β and β' Phases

MORI, Takehiko
(Tokyo Inst. Tech. and IMS)

[Bull. Chem. Soc. Jpn. 71, 2509 (1998)]

A method is proposed to systematize a number of structural modifications of BEDT-TTF (bis(ethylenedithio)tetrathiafulvalene)-based organic conductors and related materials. Analysis of actual crystal structures indicates that most crystal structures are constructed of two essential building blocks: ring-over-bond (RB) and “ring-over-atom” (RA) overlap modes. Several different ways to pile up these elements lead to various structures which are conventionally designated as β , β' , β'' , θ , α , and α' -phases (Figure 1). In the β - and β'' -phases, introduction of “dislocations” along the stacking axis generates a number of modifications, where dislocations are interactions of two donor molecules which have larger displacements along the molecular long axis than the standard RB and RA modes. Systematic nomenclature to distinguish these modifications are proposed. Transfer integrals are, however, not very sensitive to the existence of dislocations, so that the Fermi surfaces of these multiple phases are derived from the fundamental structure by folding the first Brillouin zone.

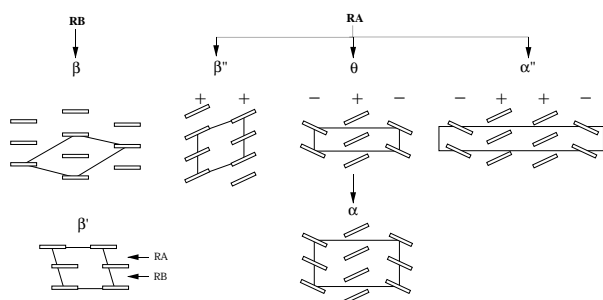


Figure 1. Genealogy of β , β' , β'' , θ , α , and α' -phases; the packing patterns of the donor sheets are viewed along the molecular long axis.

IV-Q-2 Structural Genealogy of BEDT-TTF-Based Organic Conductors II. Inclined Molecules: θ , α , and κ Phases

MORI, Takehiko¹; MORI, Hatsumi²; TANAKA, Shoji²

(¹Tokyo Inst. Tech. and IMS; ²ISTEC)

[Bull. Chem. Soc. Jpn. 72, 179 (1999)]

Overlap integrals between HOMO's of two non-parallel BEDT-TTF (bis(ethylenedithio)tetrathiafulvalene) molecules have been calculated. As the dihedral angle between the molecular planes decreases from 180° (parallel) to 90° (perpendicular), the overlap integral increases and attains a maximum around 90°. This accounts for the “universal phase diagram” of the θ -phase; θ -salts vary from an insulator to a metal with decreasing the dihedral angle (Figure 1). The ratio of the lattice constants in the conducting plane, c/a , changes in proportion to the dihedral angle. Thus c/a can be used instead of the dihedral angle. A similar universal phase diagram is applicable to analogous phases like α and α' , and also to the corresponding phases of other donors. The properties of κ -phase salts are similarly scaled by c/a . As c/a increases, the intradimer overlap integral decreases owing to the increase of the intradimer spacing, and correlated insulator, superconductor, and simple-metal phases appear in succession. When c/a increases further, another insulating phase emerges due to the decrease of the interdimer overlaps. Chemical pressure in both θ - and κ -phases reduces c/a , and stabilizes the insulating state. Hydrostatic physical pressure gives the same influence in the θ -phase, but enhances the interdimer interaction in the κ -phase to result in the opposite effect. A diagram is proposed to illustrate which structures of β , β' , θ , and κ are favored by BEDT-TTF and other donors.

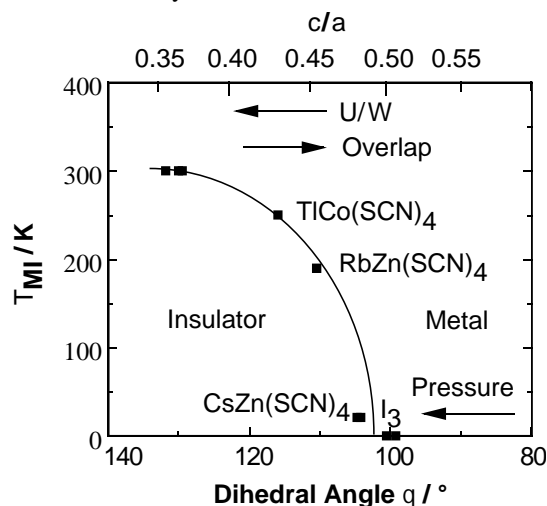


Figure 1. Universal phase diagram of the θ -phase.

IV-Q-3 $2k_F$ CDW Transition in β -(BEDT-TTF) $_2$ -PF $_6$ Family Salts

SENADEERA, G. K. Rohan¹; KAWAMOTO, Tadashi¹; MORI, Takehiko²; YAMAURA, Junichi¹; ENOKI, Toshiaki¹

(¹Tokyo Inst. Tech.; ²Tokyo Inst. Tech. and IMS)

[*J. Phys. Soc. Jpn.* **67**, 4193 (1998)]

In an attempt to clarify the nature of the metal insulator transition of β -(BEDT-TTF) $_2$ PF $_6$ family salts, temperature dependence of the static magnetic susceptibility, resistivity under various pressures, lattice parameters and the intensity of X-ray superlattice reflections have been measured for β -(BEDT-TTF) $_2$ PF $_6$ and β -(BEDT-TTF) $_2$ AsF $_6$. The transition temperature (T_{MI}) of these salts is shifted to higher temperatures with an increase of pressure. A sharp drop of the activation energy is observed at 5 kbar for the PF $_6$ salt and 6 kbar for the AsF $_6$ salt (Figure 1). Above these pressures, resistivity becomes almost flat down to low temperatures though the resistivity again increases below 50 K. Phase diagrams were constructed for both materials. Static magnetic susceptibilities of both salts exhibit abrupt drops below T_{MI} . A noticeable drop of the lattice parameters, lattice volumes and the X-ray intensities around T_{MI} indicate that the M-I transition is associated with the structural transition. The existence of the 2-fold structural changes is established by observing the superlattice reflections corresponding to (a , b , $2c$) below T_{MI} .

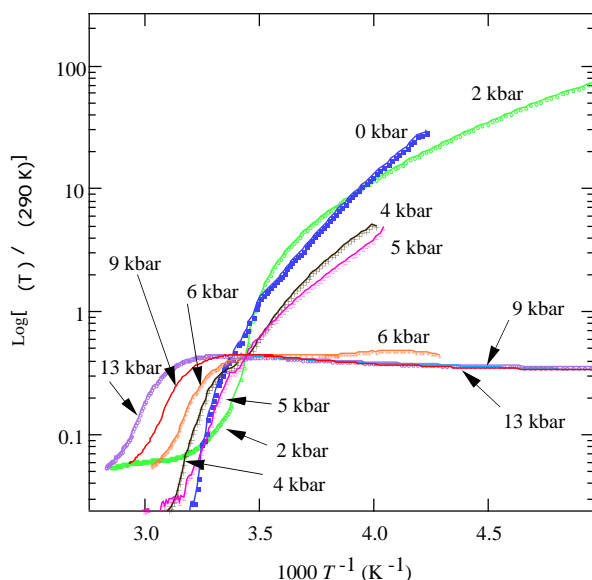


Figure 1. Temperature dependence of normalized resistivity for the PF $_6$ salt at different pressures: Arrhenius plots.

IV-Q-4 Transport Properties of α' -Phase Organic Conductors, (BEDT-TTF) $_2$ CsHg(SCN) $_4$ and (BEDT-TTF) $_2$ K $_{1.4}$ Co(SCN) $_4$

HANAZATO, Shiogo¹; MORI, Takehiko²; MORI, Hatsumi³; TANAKA, Shoji³

(¹Tokyo Inst. Tech.; ²Tokyo Inst. Tech. and IMS; ³ISTEC)

[*Physica C* **316**, 243 (1999)]

Under pressure, the metal-insulator transition temperature T_{MI} (210 K) of α' -(BEDT-TTF) $_2$ CsHg(SCN) $_4$ (BEDT-TTF: bis(ethylenedithio)tetrathiafulvalene) decreases up to 7 kbar, whereas above this pressure the system becomes more insulating as the pressure increases (Figure 1). This behavior is interpreted in view of the mixed β' -like and θ -like characters of the α' -phase. In this compound two-fold lattice modulation appears much above T_{MI} , even at room temperature. This indicates that the lattice modulation is not the direct origin of the M-I transition. In α' -(BEDT-TTF) $_2$ -K $_{1.4}$ Co(SCN) $_4$, T_{MI} (130 K) rises very slowly under pressure.

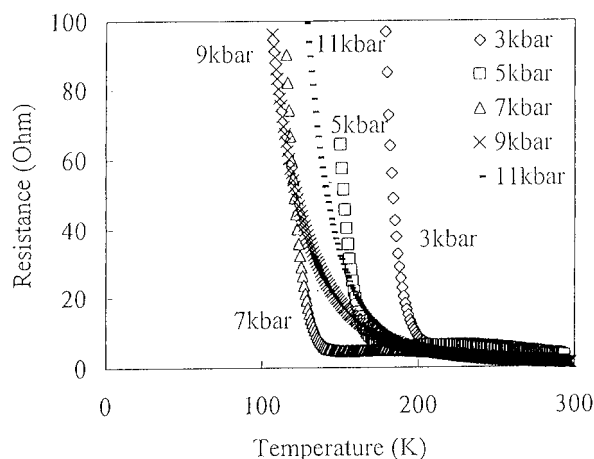


Figure 1. Temperature dependence of electrical resistance of α' -(BEDT-TTF) $_2$ CsHg(SCN) $_4$ under applied pressures.